AD-A149 699 OSCILLATOR DEVELOPMENT(U) CENTRE NATIONAL DE LA RECHERCHE SCIENTIFIQUE BESANCON (FRANCE) J J GAGNEPAIN ET AL. SEP 84 RADC-TR-84-180 1/1

UNCLASSIFIED AFOSR-82-0318 F/G 9/1 NL

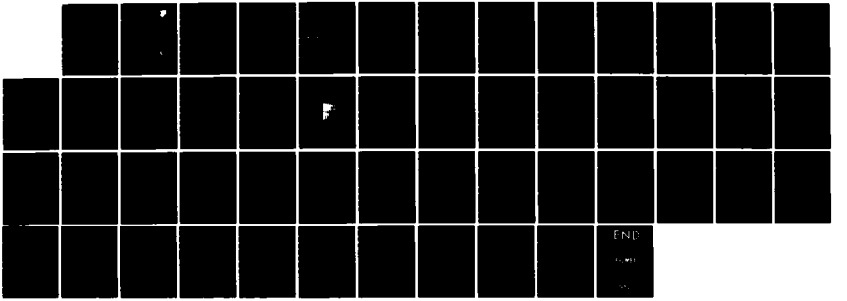

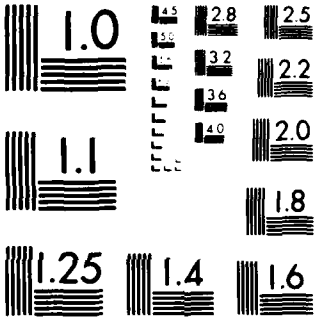

12

RADC-TR-84-180
Final Technical Report
September 1984

OSCILLATOR DEVELOPMENT

Centre National de la Recherche Scientifique Laboratoire de Physique

J. J. Gagnepain, D. Hauden and G. Theobald

APPROVED FOR PUBLIC RELEASE; DISTRIBUTION UNLIMITED

ROME AIR DEVELOPMENT CENTER
Air Force Systems Command
Griffiss Air Force Base, NY 13441

This report has been reviewed by the RADC Public Affairs Office (PA) and is releasable to the National Technical Information Service (NTIS). At NTIS it will be releasable to the general public, including foreign nations.

RADC-TR-84-180 has been reviewed and is approved for publication.

APPROVED: N. Yannoni

NICHOLAS F. YANNONI
Project Engineer

APPROVED: Harold Roth

HAROLD ROTH, Director
Solid State Sciences Division

FOR THE COMMANDER: John A. Ritz

JOHN A. RITZ
Acting Chief, Plans Office

If your address has changed or if you wish to be removed from the RADC mailing list, or if the addressee is no longer employed by your organization, please notify RADC (ESES) Hanscom AFB MA 01731. This will assist us in maintaining a current mailing list.

Do not return copies of this report unless contractual obligations or notices on a specific document requires that it be returned.

UNCLASSIFIED
SECURITY CLASSIFICATION OF THIS PAGE

REPORT DOCUMENTATION PAGE

1a. REPORT SECURITY CLASSIFICATION UNCLASSIFIED	1b. RESTRICTIVE MARKINGS N/A
2a. SECURITY CLASSIFICATION AUTHORITY N/A	3. DISTRIBUTION/AVAILABILITY OF REPORT Approved for public release; distribution unlimited.
2b. DECLASSIFICATION/DOWNGRADING SCHEDULE N/A	
4. PERFORMING ORGANIZATION REPORT NUMBER(S) N/A	5. MONITORING ORGANIZATION REPORT NUMBER(S) RADC-TR-84-180
6a. NAME OF PERFORMING ORGANIZATION Centre National de la Recherche Scientifique Laboratoir de Physique 6b. OFFICE SYMBOL (If applicable)	7a. NAME OF MONITORING ORGANIZATION Rome Air Development Center (ESES)
6c. ADDRESS (City, State and ZIP Code) Laboratoire de Physique et Metrologie des Oscillatoeurs 32, av. de l'Observatoire 25000 BESANCON, France	7b. ADDRESS (City, State and ZIP Code) Hanscom AFB MA 01731
8a. NAME OF FUNDING/SPONSORING ORGANIZATION Rome Air Development Center 8b. OFFICE SYMBOL (If applicable) ESES	9. PROCUREMENT INSTRUMENT IDENTIFICATION NUMBER AFOSR-82-0318
8c. ADDRESS (City, State and ZIP Code) Hanscom AFB MA 01731	10. SOURCE OF FUNDING NOS PROGRAM ELEMENT NO. 61102F; PROJECT NO. 2305; TASK NO. J1; WORK UNIT NO 33

11. TITLE (Include Security Classification)
OSCILLATOR DEVELOPMENT

12. PERSONAL AUTHOR(S)
J. J. Gagnepain, D. Hauden, G. Theobald

13a. TYPE OF REPORT	13b. TIME COVERED	14. DATE OF REPORT (Yr., Mo., Day)	15. PAGE COUNT
Final	FROM Aug 82 TO Aug 83	September 1984	52

16. SUPPLEMENTARY NOTATION

17 COSATI CODES			18. SUBJECT TERMS (Continue on reverse if necessary and identify by block number)		
FIELD	GROUP	SUB GR	Quartz	Noise	Fast Warm-up
09	03		Resonator	Low Temperature	Temperature
			Oscillator	Surface Acoustic Wave (SAW)	

19. ABSTRACT (Continue on reverse if necessary and identify by block number)

The objectives of this program are to: -

- Evaluate the frequency instabilities of quartz crystal resonators as a function of temperature, Q-factors and power level.
- Show the feasibility of low temperature quartz oscillators. ....
- Determine the dynamic thermal behavior of SAW quartz oscillators and determine crystal orientation and wave propagation directions with minimized sensitivities. -

(A) - A new series of noise measurements versus Q-factors was performed at room temperature on quartz resonators of different types. The influence of power levels was studied up to powers corresponding to chaotic states.

20. DISTRIBUTION/AVAILABILITY OF ABSTRACT	21. ABSTRACT SECURITY CLASSIFICATION
UNCLASSIFIED/UNLIMITED ☐ SAME AS RPT ☒ DTIC USERS ☐	UNCLASSIFIED

22a. NAME OF RESPONSIBLE INDIVIDUAL	22b. TELEPHONE NUMBER (Include Area Code)	22c. OFFICE SYMBOL
Nicholas F. Yannoni	(617) 861-2???	RADC (ESES)

DD FORM 1473, 83 APR EDITION OF 1 JAN 73 IS OBSOLETE

UNCLASSIFIED
SECURITY CLASSIFICATION OF THIS PAGE

- Short and medium term frequency stabilities were measured at liquid helium temperature using dual crystal passive systems.

- A quartz oscillator was designed for operation in liquid helium.

(B) - The dynamic temperature of SAW oscillators was calculated using two different approaches in bi-dimensional model.

- In the first one thermoelastic coupling between bending and extensional forces was neglected. Sensitivities were rather small and not so realistic.

  In the second one all thermoelastic coupling was considered.

- Frequency-temperature characteristics were simulated for different crystal orientations taking into account the rate of temperature change and the phase difference between the internal temperature (effective temperature) and the external temperature (temperature given by a probe in an experiment).

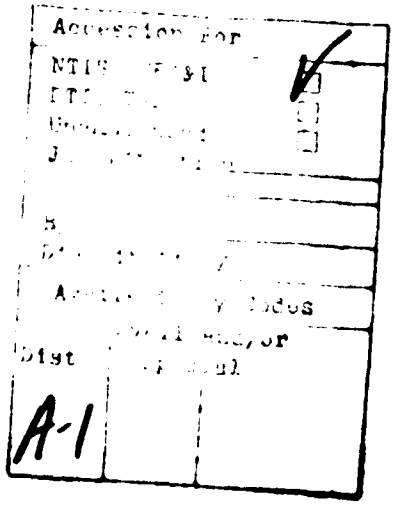

OSCILLATOR DEVELOPMENT

Table of contents

CONTRIBUTIONS

Contributions to various parts of the program were made by the following persons

J. Groslambert, C. Paulin, members of the technical staff of LPMO

G. Robichon, Ing. at Compagnie d'Electronique et de Piézoélectricité (CEPE - Argenteuil, France) presently at LPMO.

I - LOW TEMPERATURE QUARTZ CRYSTAL OSCILLATOR

GENERAL PRESENTATION

One of the main results regarding 1/f noise obtained during this program was the $1/Q^4$ dependance law. A new series of noise measurements was performed on different kinds of resonators to confirm this law and principally to study the influence of power level on the noise behavior. Comparative measurements were achieved at low, medium and high powers. A new result is the possibility for quartz resonators to experience chaotic behavior.

Frequency stability at low temperature was measured at both short and medium terms using the dual crystal passive system. Comparisons are made with corresponding stabilities of the same crystal measured at room temperature in the same system.

Realization of an oscillator at low temperature, including crystal and electronics, is discussed, and preliminary results are given.

1/f NOISE LEVEL VERSUS POWER LEVEL

1) Noise at low power *

The measurement system remains the same and details can be found in previous reports (AFOSR grants 80-0105 and 81-0191).

2.5 MHz, 5 MHz and 10 MHz crystals were measured.

* These measurements were performed at the National Bureau of Standards Frequency and Time Division by J.J. Gagnepain.

1) 5 MHz resonators. Six AT-cut crystals (5th overtone) were studied. Two were commercial BVA resonators and four were standard commercial high quality resonators. A typical spectrum (pair of BVA crystals) is shown in Fig. 1. The noise is essentially 1/f frequency noise. The $1/f^3$ noise is due to the filtering effect of the resonator ; this occurs at its half bandwidth. For three pairs of resonators the frequency noise $S_y^{1/2}(f)$, measured 1 Hz from the carrier were equal to $2.5 \times 10^{-13}/\sqrt{Hz}$, $2.5\times10^{-13}/\sqrt{Hz}$ and $3\times10^{-13}/\sqrt{Hz}$. The raw data were divided by $\sqrt{2}$ under the assumption that the noise of each resonator was identical. Obviously by doing all possible pairs one can obtain a more accurate value for each resonator independent of this assumption. All these resonators had unloaded Q-factors in the range $2.5\times10^6 < Q_o < 2.7\times10^6$.

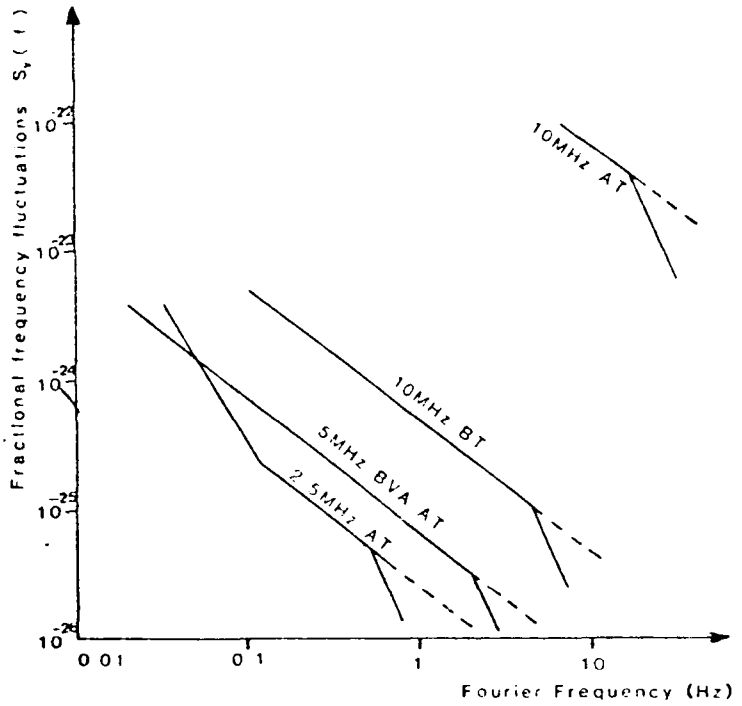

Fig. 1
The solid curve shows the apparent frequency noise spectrum of 2.5 MHz, 5 MHz and 10 MHz resonators. At Fourier frequencies above the half bandwidth, the spectrum must be corrected for the filtering effect of the resonators yielding the dashed lines.

2) 10 MHz resonators. Two kinds were measured : AT-cut and BT-cut crystals. Both were third overtone resonators, but with very different Q-factors, typically 3×10^5 for AT-cut and 1.7×10^6 for BT-cut. BT-cut crystals have much higher Q-factors because this crystallographic orientation has lower internal losses for the thickness-shear mode.[1] Noise spectra are shown in Fig. 1. A large difference in the noise levels can be observed between the AT and BT cuts. At 1 Hz from the carrier these levels are of the order of $7\times10^{-3}/\sqrt{Hz}$ for the BT resonators to $3.2\times10^{-11}/\sqrt{Hz}$ for the AT resonators. These results show a strong dependence between the 1/f noise level and Q-factor.

3) 2.5 MHz resonators. Two pairs of fifth overtone, AT-cut resonators were tested with unloaded Q-factors close to 4×10^6. Although these pairs had almost the same Q-factors, the noise levels differed by almost one order of magnitude. The presence of $1/f^2$ noise in the spectra of $S_{y_o}(f)$ indicates that the sensitivity to temperature fluctuations are very large for this type of resonator.

All the resonators were measured at powers of the order of 10 μW.

The 1/f noise power 1 Hz from the carrier, evaluated for each individual crystal, was plotted as a function of the unloaded Q-factors in Fig. 2. A linear regression among these experimental points gives

$$S_{y_o}(1\ \text{Hz}) \approx \frac{2}{Q^4}$$

These results are also summarized in Table I.

The data show a clear dependence of 1/f noise on the resonator's unloaded Q-factors, following a $1/Q^4$ law. The only exception is with the 2.5 MHz (#2) crystals, which show excessive noise most likely due to thermal transient effects.

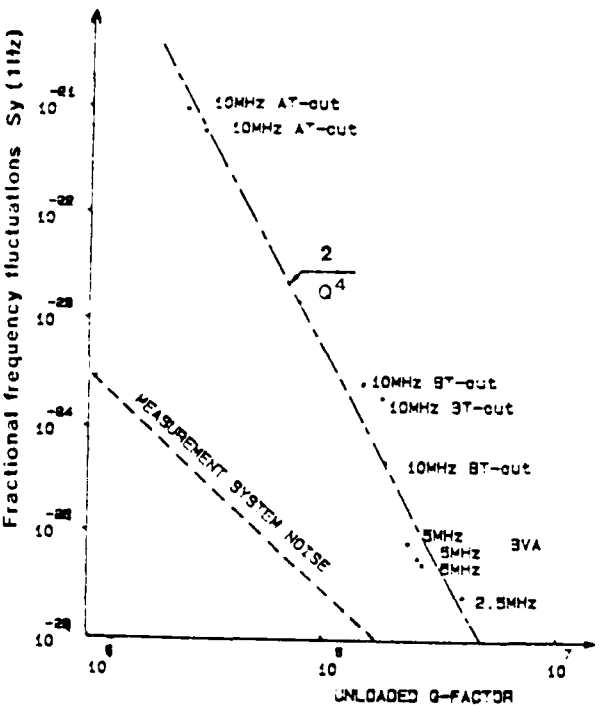

Fig. 2
1/f noise level, measured at 1 Hz from the carrier as a function of the unloaded Q-factor for the different resonators tested. The measurement system noise is indicated by ----

If these crystals are used in an oscillator, the 1 f spectrum will give a flicker floor in time domain, whose corresponding values are given in Table I, and which corresponds to the best stability achievable in that case with an oscillator, at least at room temperature.

resonator	2.5 MHz # 1	2.5 MHz # 2	5 MHz	5 MHz	5 MHz	10 MHz	10 MHz	10 MHz	10 MHz	10 MHz
crystal cut	AT	AT	AT	AT	AT	AT	AT	BT	BT	BT
Q_o	4.10^6	4.10^6	$2.6.10^6$	$2.7.10^6$	$2.4.10^6$	$2.5.10^6$	3.10^5	$1.5.10^6$	$1.8.10^6$	$1.9.10^6$
S_y 1 Hz	$2.5.10^{-26}$	$2.4.10^{-24}$	$6.2.10^{-26}$	$5.8.10^{-26}$	9.10^{-26}	1.10^{-21}	$6.5.10^{-22}$	$2.5.10^{-24}$	2.10^{-24}	$1.3.10^{-25}$
flicker floor	$1.9.10^{-13}$	$1.5.10^{-12}$	$2.9.10^{-13}$	$2.8\ 10^{-13}$	$3.5.10^{-13}$	$3.7.10^{-13}$	$3.0.10^{-13}$	$1.9.10^{-12}$	$1.7.10^{-12}$	$1.3.10^{-13}$

Table I

1/f noise level at 1 Hz from the carrier, and corresponding flicker floor, for the different samples
2.5 MHz # 2 crystals were not taken into account in the linear regression of Fig. 2

2) **Noise at medium power**

When the drive level of the crystal is increased it exhibits nonlinear effects due mainly to the higher order elastic constants. This is the well known amplitude frequency effect where distortions appear in the amplitude and phase resonance curves and even hysteresis can be developed as shown in Fig. 3.

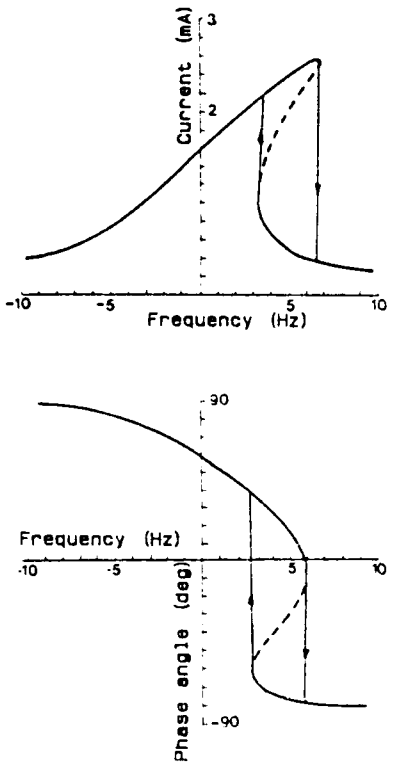

Fig. 3
Amplitude and phase resonance curves of quartz resonators

The nonlinear behavior of a resonator driven in transmission can be represented by the phenomenological relation

$$\frac{d^2 i}{dt^2} + \frac{\omega_0}{Q}\frac{di}{dt} + \omega^2\left[1 - 2\varepsilon(\Omega)\cos\Omega t\right] \times i(1 + ki^2) = F\cos\omega t$$

where i is the current through the crystal, Q the loaded Q-factor, and F the amplitude of the driving force. k is the nonlinear coefficient (related to the next higher order elastic constants). $\varepsilon(\Omega)\cos\Omega t$ introduces a modulation of the resonance angular frequency ω_0, which represents the frequency noise of the resonator. Solving this equation with a perturbation method gives the phase noise of the output signal.

Let $S_{y_0}(\Omega)$ be the frequency noise spectrum of the crystal. When driving it at low power, in the linear range, the corresponding phase spectrum is given by

$$S_\phi(\Omega) = S_{y_0}(\Omega)\,\frac{\omega_0^2}{\Omega^2 + \omega_0^2/4Q^2}$$

At medium levels, when the resonator is driven near the jump frequency, the phase spectrum becomes

$$S_\phi(\Omega) = S_{y_0}(\Omega)\,\frac{\omega_0^2(\Omega^2 + \omega^2/4Q^2)}{\Omega^2\,(\Omega^2 + \omega_0^2/Q^2)}$$

Thus the ratio between the phase noise at medium and low powers is

$$\frac{S_\phi(\text{high power})}{S_\phi(\text{low power})} = \frac{(\Omega^2 + \omega_o^2/4Q^2)^2}{\Omega^2(\Omega^2 + \omega_o^2/Q^2)}$$

This ratio goes to unity for $\Omega \gg \omega_o/Q$ and is equal to $\omega_o^2/16Q^2\Omega^2$ for $\Omega \ll \omega_o/4Q$. Therefore the induced phase noise for the lower Fourier frequency components can be greatly increased by the crystal nonlinearities. Such a noise was experimentally observed on a 5 MHz (5th overtone AT-cut) resonator driven at 2.5 mW, as shown on Fig. 4.

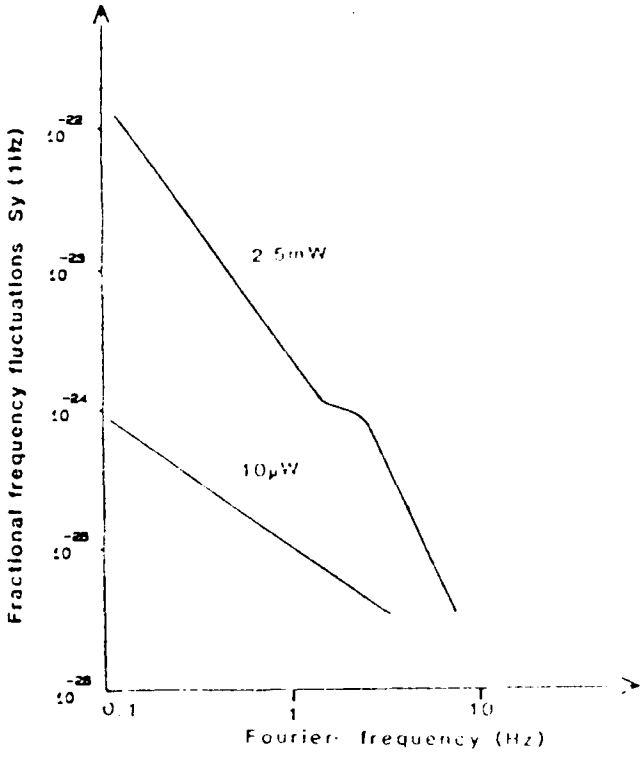

Fig. 4
Frequency noise spectrum of a 5 MHz driven at low and medium power

3) Noise at high power

At still higher power (of the order of a few watts) the quartz resonator was found to exhibit large instabilities as shown in Fig. 5.

Such phenomena are known in nonlinear systems as chaotic behavior. Chaos has been observed in many different systems[2], for example phase locked loops[3] and Josephson junctions [4,5] which can be considered as low Q-factor resonators. The main difference between these systems and quartz crystal resonators stem from the high Q-factor and thermal effects, which strongly modify the behavior of the crystal at high power.

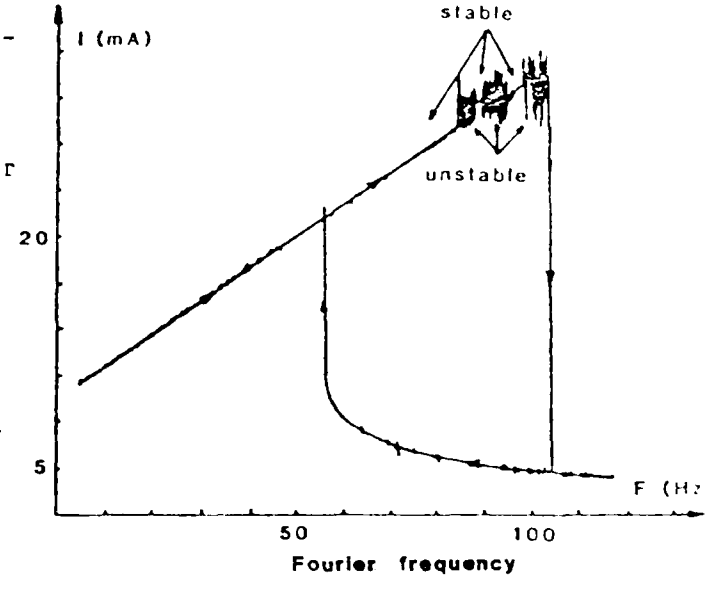

Fig. 5
Stable and unstable states of a 5 MHz resonator driven at high power

Thermal effects will be predominant mainly if the crystal is operated at a temperature below its turnover temperature. In this case the temperature coefficient is negative (of the order - 4 Hz/°C). The temperature rise due to the dissipated power induces a negative frequency shift, which can be large enough to pull the crystal frequency to the frequency where the down-jump phenomenon occurs (Fig. 3). Thus the amplitude becomes much smaller decreasing the dissipated power. Temperature therefore decreases causing the frequency to increase until it reaches the second jump and so on. This gives a cycling with large amplitude and phase perturbations, as shown in Fig. 6. This phenomenon occurs when the amplitude-frequency effect and the temperature coefficient have opposite signs.

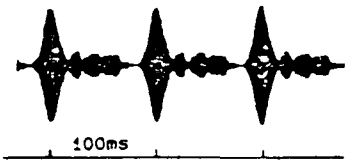

Fig. 6
Amplitude perturbation due to thermal effects at high power

Above the turn-over temperature the sign of the temperature coefficient becomes positive. In this case the temperature rises, inducing a positive frequency change, which corresponds to an additional amplitude-frequency effect. This is equivalent to increasing the nonlinearities of the crystal.

Fig. 5 illustrates the amplitude resonance curve of a 5 MHz (AT-cut, fifth overtone) crystal excited with a 7 V rms driving signal. As the drive frequency increases the crystal goes from stable state to chaotic states through sudden transitions.

This is quite different from the behavior of low-Q resonant systems. For the latter the route to chaos goes through a set of cascading subharmonic bifurcations. The rate at which the number of subharmonics increases with driving power leads quickly to a spectrum composed of so many spectral lines that it appears as a continuous noise spectrum.

For high Q resonators, like quartz resonators, subharmonic generation is not observed because all these subharmonic frequencies are out of the resonator bandwidth and therefore filtered. Only when their number is large enough, such as when there are components in the resonator bandwidth, chaotic behavior appears. This explains the sudden transition to chaos without observation of cascading bifurcations.

The sideband frequency noise of the transmitted signal was measured under the same conditions as at low and medium powers. A f^2 spectrum is observed for the power spectral density of the frequency fluctuations of the signal. This corresponds to a white phase spectrum and therefore to white noise for the frequency fluctuations of the crystal. This is in agreement with other observations of chaos[2-5], but does not lead to 1/f noise. This is shown in Fig. 7.

The level of this noise is 10^{-18} (power spectral density) and is to be compared with the level of Fig. 1. The noise is increased by several orders of magnitude.

These results confirm the $1/Q^4$ law of the 1/f noise level, and this is shown quite clearly by comparing crystals at the same frequency but with very different Q-factors such as AT and BT crystals. 1/f noise can be altered and magnified by the nonlinear response of the crystal as has been shown at medium power. At high power, large noise is generated, but this noise is not related with the previous one, and the exhibited spectrum is purely white.

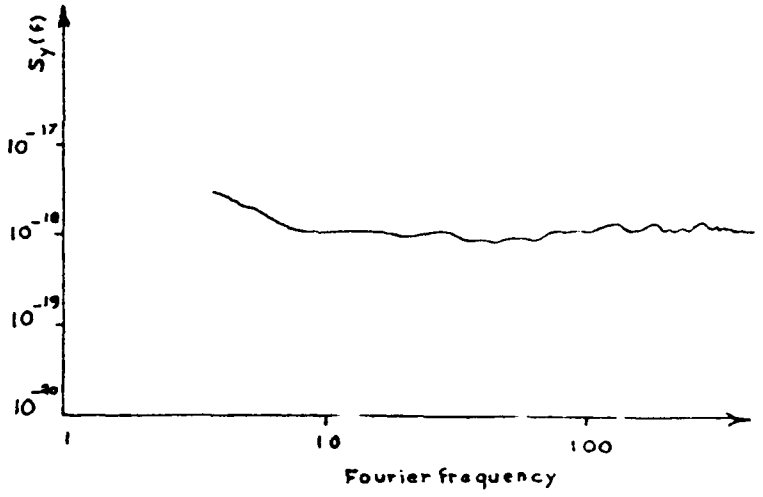

Fig. 7
Frequency fluctuations of a 5 MHz resonator driven at 7 VRMS illustrating the chaotic state of the crystal

LOW TEMPERATURE DUAL CRYSTAL PASSIVE SYSTEM

The dual crystal passive system which is used allows operation of a crystal at low temperature while keeping the electronics at room temperature. This system was described in the previous report, and only the schematic diagram is presently recalled.

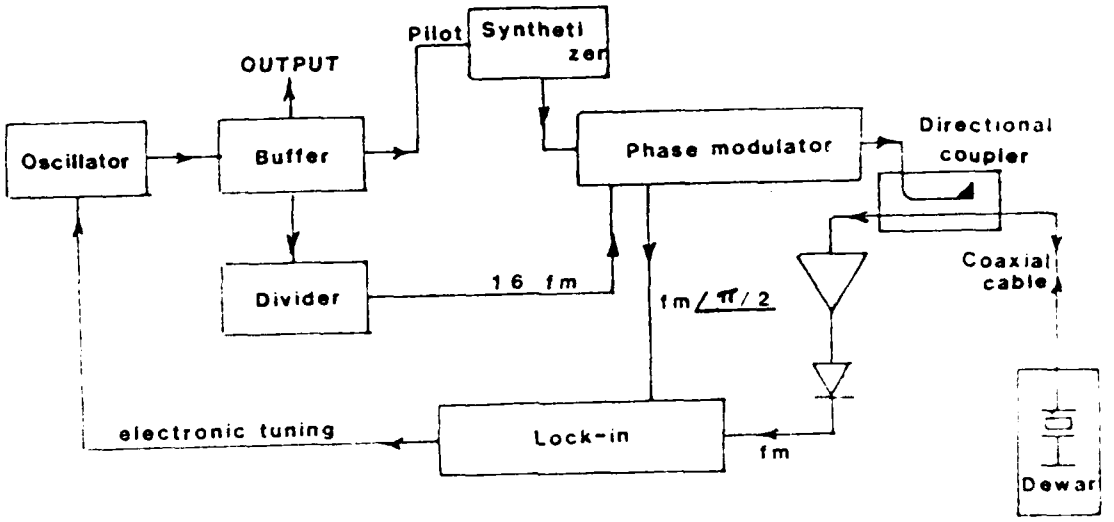

Fig. 8
Schematic diagram of dual crystal passive system

This system was tested first at room temperature. When operating at low temperature the main difference comes from the long link, a coaxial cable, between the electronics and the crystal respectively outside and inside the dewar.

The phase loop which locks the active oscillator to the passive resonator acts as a discriminator.

The overall response was tested in real conditions. Quite different behavior was observed from room to low temperature, as shown in Fig. 9a and 9b.

The spurious responses observed at low temperature are due to VSWR induced by mismatching between the 50 Ω characteristic impedance of the coaxial cable and the motional impedance of the crystal which can become as low as a few ohms, when at low temperature.

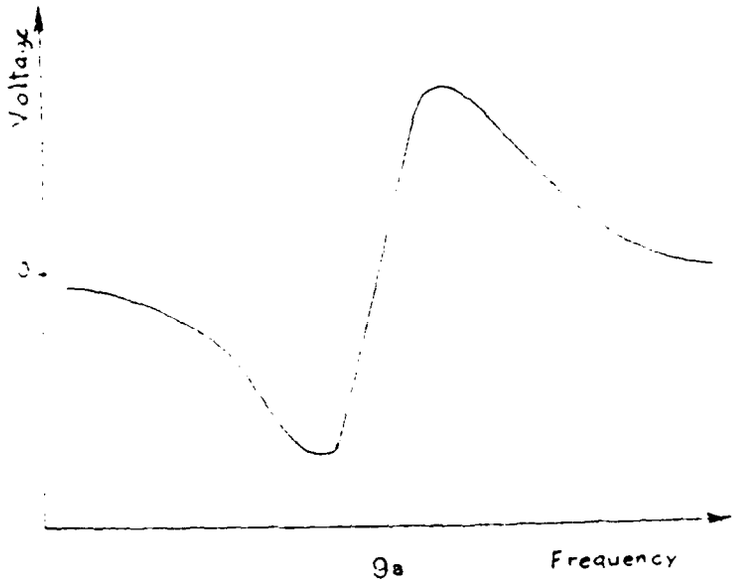

9a

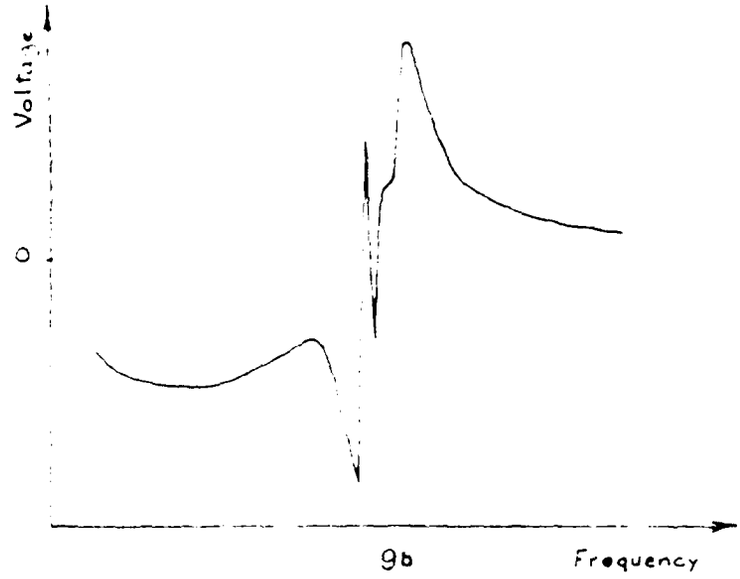

9b

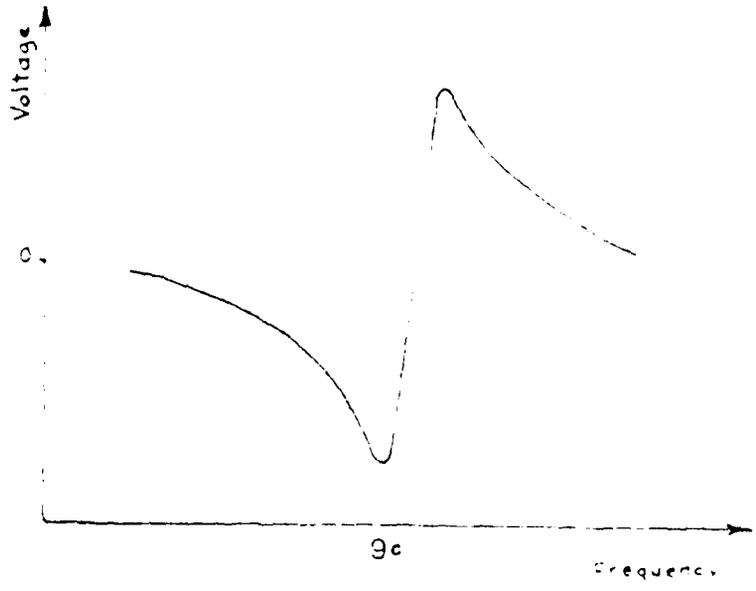

9c

The spurious responses could be avoided in principle by using a small-size wideband RF transformer, but no such transformer was able to be operated in liquid helium with sufficient efficiency. This is due to the ferrite core which looses its magnetic properties at cryogenic temperatures.

The problem was solved by introducing a serial resistor in the crystal circuit, even if it is not the most satisfactory solution. The response is given in Fig. 9c.

The dynamic thermal behavior of the crystal was studied at low temperature. The frequency-temperature characteristic is represented by the well known relation

$$\Delta f/f = a_0(T-T_0) + b_0(T-T_0)^2 + \ldots + \tilde{a}\, dT/dt$$

where a_c, b_c and $\tilde{a}$ are the static and dynamic temperature coefficients.

The dynamic coefficient was evaluated by modulating the temperature of the oven inside the helium bath at .1 Hz and recording the corresponding frequency change. As shown on Fig. 10 the phase difference between the two signals is small. This indicates also a small dynamic effect. Therefore the exact value of $\tilde{a}$ cannot be exactly measured, but its upper limit was evaluated yielding

$$\tilde{a} < 6\times10^{-10}\ s/K$$

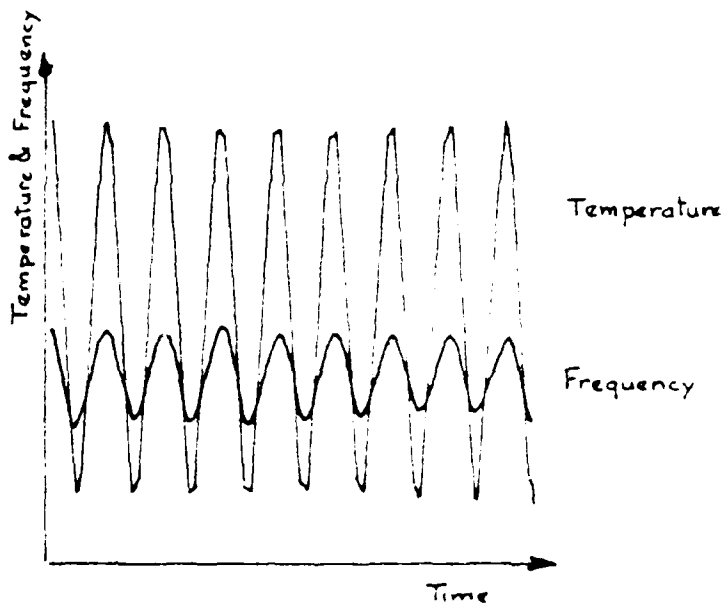

Fig. 10 : Temperature and frequency variations

At the same time the static coefficient a_0 was measured. Near 1.5 K its value was

$$a_0 = 2\times10^{-9}\ /K$$

The resonator under test was a 5 MHz, 5th overtone AT-cut crystal. Its static F-T characteristic is given in Fig. 11.

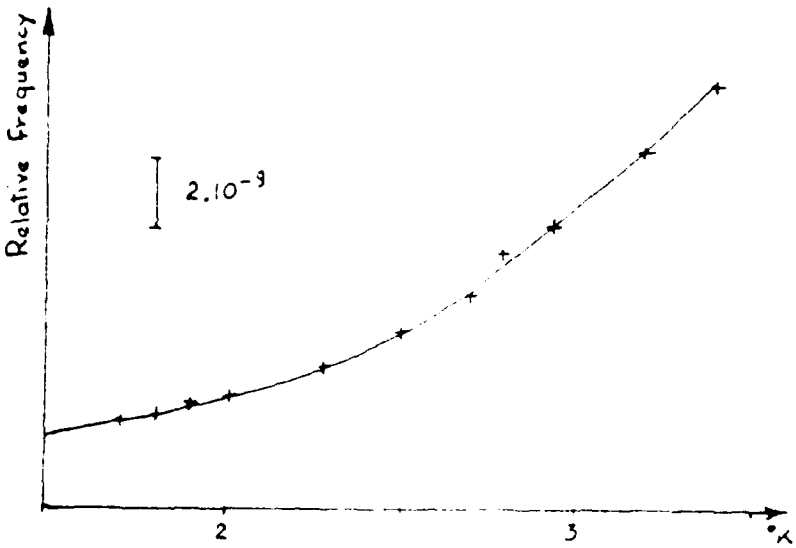

Fig. 11 : Frequency-temperature static characteristic of a 5 MHz, 5th overtone, AT- cut resonator

Short term frequency stability was measured by simultaneous comparison with different high stability crystal oscillators. This "triangulation" method has an equivalent resolution which is of the order of 2×10^{-14} over 100 s.

Medium term frequency drift, i.e. over one day, was obtained by comparison with a Cs clock. It was not possible to test the frequency drift over more than one day, because low temperature in the dewar cannot be maintained for larger periods of time without refilling.

Stabilities of the crystal are given in table II and can be compared to the corresponding stabilities of the same crystal when operated at room temperature.

	T = 1,5 K	T = 300 K	
σ_y (10 s)	8×10^{-13} (BW=1KHz)	3×10^{-12}	drift
σ (100 s)	3×10^{-13}	3×10^{-12}	removed
drift	$< 10^{-11}$/day	2×10^{-10}/day	

Table II
Comparative stabilities of the 5 MHz, 5th overtone AT-cut crystal under test

At room temperature the 2×10^{-10}/day drift was observed after one week of oscillation. This value is not characteristic of a very high stability crystal. But improvement by more than one order of magnitude is obtained at low temperature. And in this case frequency was recorded as soon as the crystal has been cooled down, without any preageing.

A short term improvement is also about one order of magnitude, and the limitation is still due to residual temperature fluctuations acting outside on the electronics.

CRYOGENIC OSCILLATOR

Components

Different components were selected as a function of their behavior at low temperature.

a) Resistors

Metal film resistors were used. The low temperature behavior depends on its history. After a first cooling (into liquid nitrogen) a drift of 3×10^{-4}/hour was observed with a 30 kΩ resistor. Temperature cycling is necessary to stabilize the resistor.

b) Diode

A germanium diode was studied at 1.2 °K. The tension V_D which is 0.7 V at 300 °K takes the value of 10 V at low temperature as shown on Fig. 12.

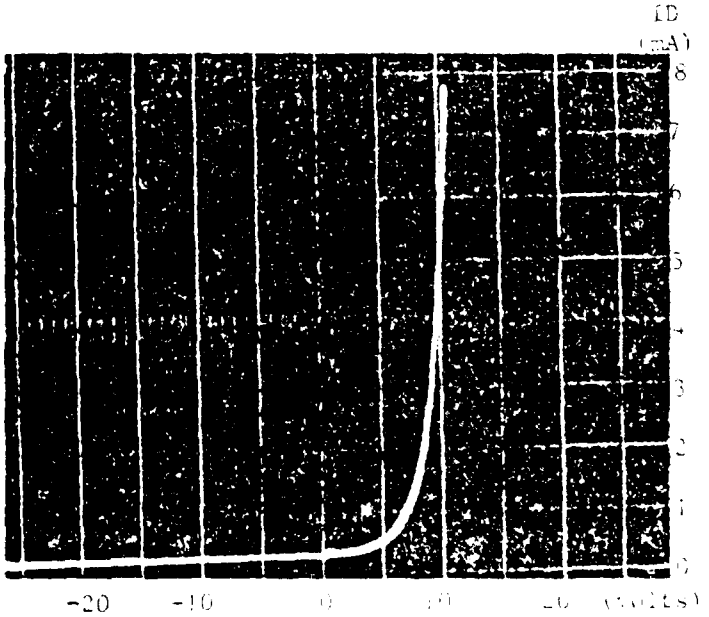

Fig. 12

Characteristics of GEC 2AG diode at 1.2 K

c) Transistors

N-channel, dual gate, MOSFET, transistors are the most appropriate ones for operating at low temperature.

As observed on Fig. 12a, b, c, they are improved at low temperature.

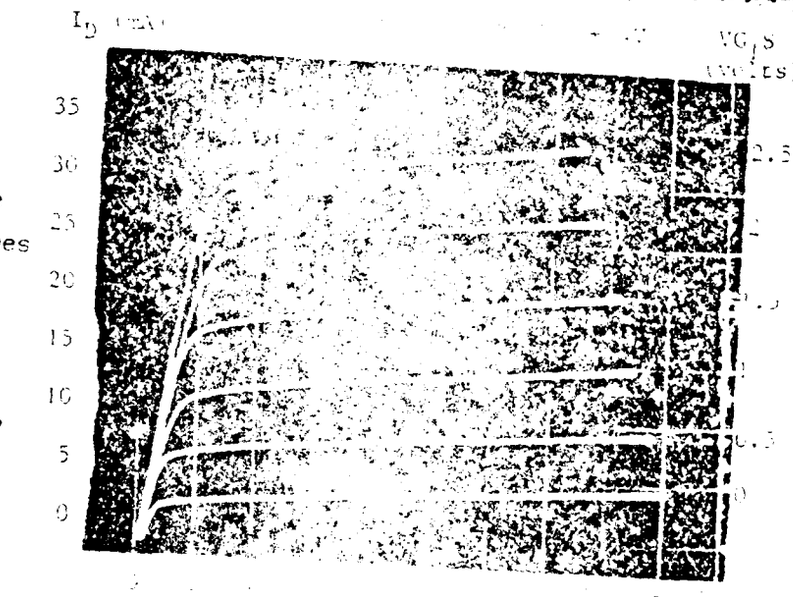

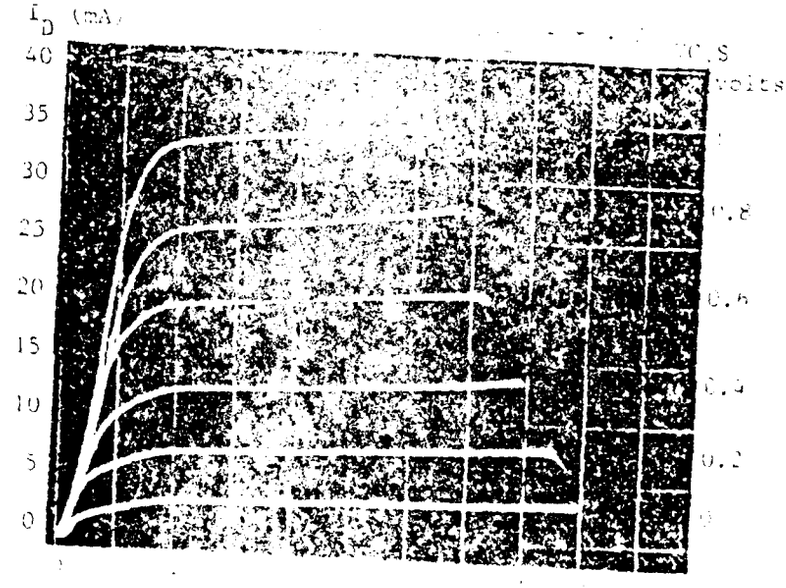

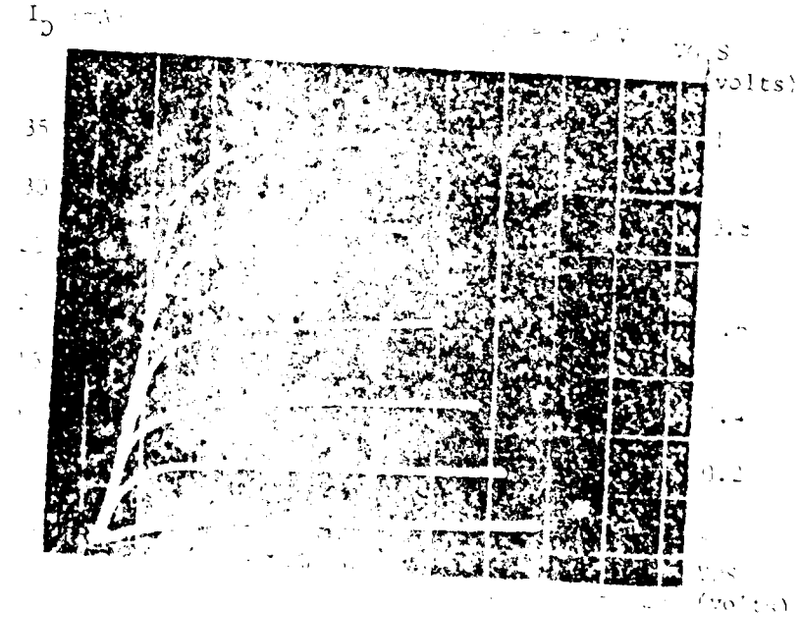

Oscillator

A Colpitts-type-oscillator was chosen with a dual gate MOSFET transistor [7]. The second gate is used to control the excitation level (Fig. 13). This oscillator was operated at 1.2 °K.

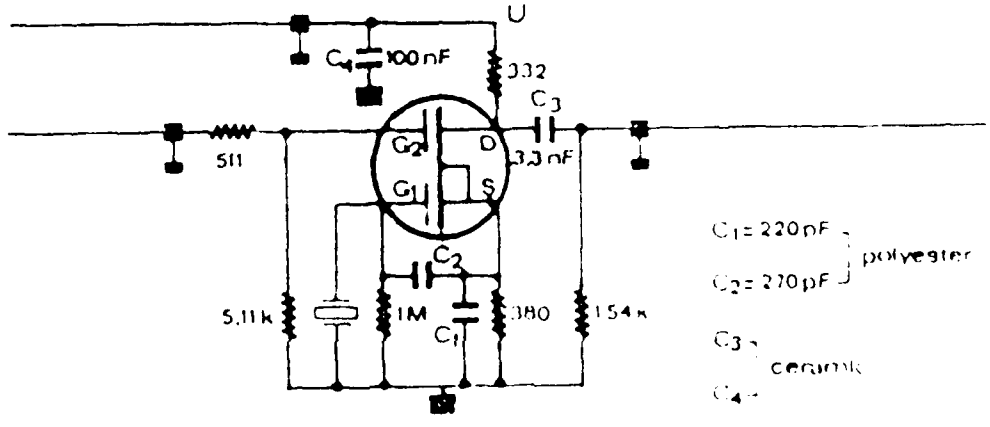

Fig. 13

Oscillation level must also be controlled using AGC.

Fig. 14 shows the dependence of the output frequency on the gate n°2 tension level. In order to improve the frequency stability, it is necessary to reduce the oscillation level as much as possible.

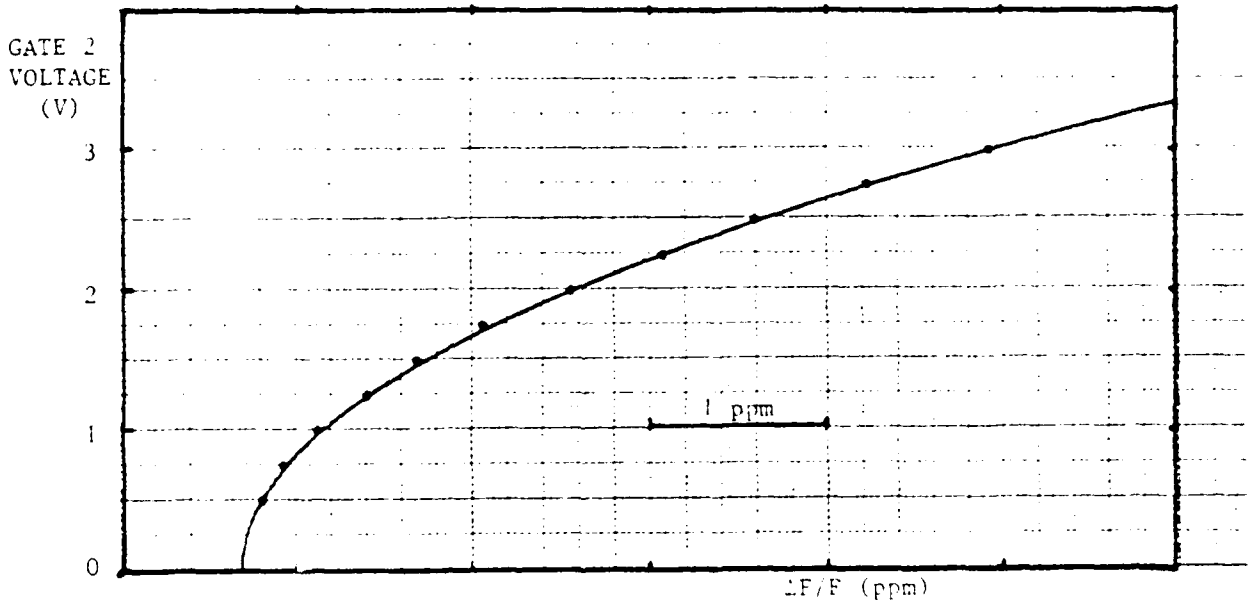

Fig. 14

These results are preliminary. The oscillator is now in operation and frequency stability measurements will be in progress in the near future.

GENERAL CONCLUSIONS

Two aspects were examined during the three steps of this grant

- the noise behavior of quartz crystal oscillators

- the feasibility and performance of a low temperature quartz frequency standard.

a) Two different noise phenomena are observed in the fluctuations of the resonance frequency of a quartz resonator.

- $1/f^2$ random walk noise which is quite well understood and can be attributed to temperature fluctuations.

- 1/f flicker noise, which is the main object of the study. A clear correlation of 1/f noise with the unloaded Q-factor, i.e. the internal acoustic loss, was found. The $1/Q^4$ dependence law was explained theoretically by the assumption of fluctuations in the thermal phonon relaxation time constant. This important result can be a guideline for the complete understanding of 1/f noise ! The main point which remains to be demonstrated is a 1/f noise spectrum in the fluctuations of the phonon time constant ; this presupposes the calculation of this time constant which has not yet been done.

On the other hand, the influence of impurities was also studied. It was shown that fluctuations of their relaxation time constants can also lead to $1/Q^4$ dependance law. It remains to be shown experimentally that impurity relaxation contributes to the general 1/f noise behavior of the crystal. This would be possible by measurement of 1/f noise at 50 K for instance at the maximum of Na^+ ion relaxation.

Finally the noise behavior was examined at high powers, when the crystal becomes strongly nonlinear and experiences chaotic behavior. A very large noise increase was observed. This noise has a white spectrum and apparently does not lead to 1/f.

b) The measurements of frequency stability of a quartz crystal resonator and/or oscillator at low temperature were mainly performed by using the concept of a dual crystal passive system, i.e. a passive quartz resonator in liquid helium and a phase locked oscillator at room temperature. This supposed:

- accurate temperature control in the helium bath
- low noise electronics
- minimization of cable effects
- study of the properties of quartz at low temperature.

The results obtained with a medium quality quartz crystal exhibited improvement of both short (10-100s) and medium (1 day) term stabilities by one order of magnitude, and this without any preaging.

Stabilities in the range of a few parts in 10^{-14} at short term and 10^{-12} per day seem to be feasible with high quality crystals. Right now this supposes principally a better stability of the electronics at room temperature.

The realization of a complete oscillator in liquid helium was undertaken. The advantage is simplicity and the avoidance of external effects at room temperature. The oscillator is made and stability measurements are in progress, but results were not yet available for inclusion in this report.

As a brief summary, the following points are considered as the main results of the program :

- 1/f noise in quartz crystals is related to acoustic attenuation ;
- it follows a $1/Q^4$ law ;
- assumption is made of fluctuations of thermal phonon relaxation time constants ;
- impurities can contribute to 1/f behavior ;
- operating a quartz resonator at low temperature improves both short and medium term stabilities by at least a factor 10.

REFERENCES

(1) J. Lamb and J. Richter, "Anisotropic acoustic attenuation with new measurements for quartz at room temperatures", Proc. Roy. Soc. A, vol. 293, p. 479 (1966).

(2) "Evolution of order and chaos", Proc. Int. Symp. on Synergetics. H. Haken Ed. Springer-Verlag (1982).

(3) D. D'Humieres, M. Bearley, B. Huberman, A. Libchaber, "Chaotic states and routes to chaos in the forced pendulum", Ginzton Lab. Report 33429, Stanford University (1982).

(4) B.A. Hubertson, J.P. Cratchfield, "Chaotic states of anharmonic systems in periodic fields", Phys. Rev. Letters, 43, n° 23, p. 1743 (1979).

(5) M. Petersen, A. Davidson, "Chaos and noise rise in Josephson junctions", Appl. Phys. Lett., 39, n° 10, p. 830 (1981).

(6) A. Ballato, J.R. Vig, "Static and dynamic frequency-temperature behavior of singly and doubly rotated oven-controlled quartz resonator", 32nd An. Freq. Cont. Symp. (1978).

(7) G. Mossuz, J.J. Gagnepain, "Quartz crystal oscillator at very low temperature", Cryogenics, (1976).

GENERAL PRESENTATION

When a quartz crystal plate is subject to a change of the ambient temperature, it undergoes a time-dependent inhomogeneous temperature distribution which causes perturbation of the frequency. This is called dynamical thermal behavior. In bulk resonators, cuts are found which are not sensitive to varying temperature.

The purpose of the present study is to determine the dynamical behavior in SAW oscillators. In thin quartz plates, thermal diffusion is deemed predominant in one direction. This leads to a one dimensional model which was presented in a previous report (June 1982). It appears however that in a finite plate, diffusion along another direction could modify the temperature representation and the spatial repartition of stresses. The time-dependent inhomogeneous two-dimensional temperature distribution in the quartz is obtained from the uncoupled heat conduction equation subject to the appropriate boundary conditions. Since the heat conduction is sufficiently slow compared to the speed of elastic waves, the mechanical inertia terms can be neglected in the stress equation of motion, reducing them to the quasi-static stress equations of equilibrium. The time-dependent, thermally-induced deformation state is obtained from the static linear thermoelasticity.

A perturbation analysis of the equilibrium equations for small vibrations superposed on the static thermal bias has been performed.

The resulting changes in wave velocity show that dynamic thermal behavior of SAW devices is governed by two terms :

- the first resulting directly from the thermal gradients within the crystal is proportional to the temperature perturbation. It can be described by a coefficient $\bar{a}$ and it points out the effect of a temperature perturbation which is time-dependent or time-independent.
- the second one, related linearly to the time rate of change of measured temperature, introduces the dynamic thermal coefficient $\tilde{a}$.

THERMOELASTIC THEORETICAL MODELS

1) Two-dimensional temperature distribution

A diagram of the crystal plate is shown in Fig. 1 along with the associated coordinate system.

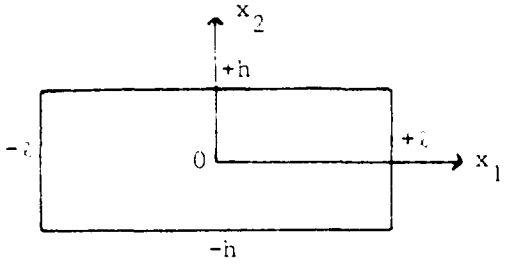

Fig. 1
Cross section of the plate

The x_2 coordinate axis is normal to the major surfaces of the plate. The length of the plate in the Ox_3 direction is large compared with the cross sectional dimensions ($2h \times 2\ell$).

We discuss two special cases of heating which could represent experimental thermal perturbations.

Case I : Lateral heating

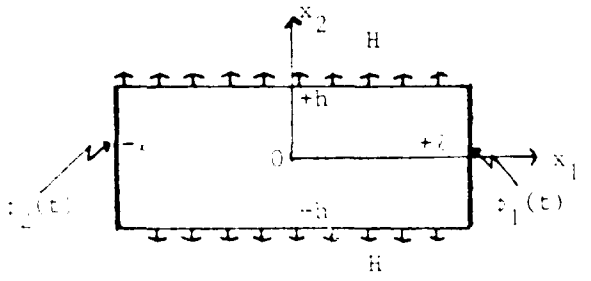

Fig. 2

Schematic diagram of the plate heating on both lateral surfaces. Heat transfer occurs at the $x_2 = \pm h$ faces

The first case was mentioned in the previous report. Prescribed surface temperatures $\Phi_1(t)$ and $\Phi_2(t)$ are at the end faces $x_1 = +\ell$ and $x_1 = -\ell$ (Fig. 2). A linear heat transfer with the ambient medium at zero temperature occurs at the major faces $x_2 = \pm h$. Temperature $\theta(x_1, x_2, t)$ inside the plate is governed by the following equations

$$\frac{\partial^2\theta}{\partial x_2^2} + \frac{\partial^2\theta}{k^2\partial x_1^2} - \frac{1}{\kappa}\frac{\partial\theta}{\partial t} = 0 \qquad \begin{matrix} -h < x_2 < h \\ -\ell < x_1 < \ell \end{matrix} \qquad (1a)$$

$$\begin{matrix} \theta = \Phi_1(t) & x_1 = +\ell & -h < x_2 < h \\ \theta = \Phi_2(t) & x_1 = -\ell & -h < x_2 < h \end{matrix} \qquad (1b)$$

$$\pm \lambda_2 \frac{\partial \theta}{\partial x} + H\theta = 0 \qquad x_2 = \pm h \qquad -\ell < x_1 < \ell \tag{1c}$$

$$\theta(x_1, x_2, 0) = 0 \qquad \text{at } t = 0 \tag{1d}$$

$k^2 = \lambda_2/\lambda_1$ is the ratio of the thermal conductivities in the x_2 and x_1 directions. κ is the thermal diffusion constant in the x_2 direction and H is the linear heat transfer coefficient.

The analytical solution of the diffusion equation (1a) along with the initial condition (1d) and boundary conditions (1b-1c) is deduced from the analytical solution obtained with Φ_1 and Φ_2 considered as time-independent, by Duhamel's theorem [1]. The result is

$$\theta(x_1,x_2,t) = \sum_n 2Hh \frac{\cos \alpha_n x_2}{\cos \alpha_n h} \frac{1}{(\alpha_n^2+H^2)h^2 + Hh}$$

$$+ \left(\Phi_1(t) \frac{\sinh k\alpha_n(x_1+\ell)}{\sinh k\alpha_n 2\ell} + \Phi_2(t) \frac{\sinh k\alpha_n(\ell-x_1)}{\sinh k\alpha_n 2\ell}\right. \tag{2}$$

$$\left. - \sum_{i=1}^{\infty} (-1)^{i+1} \frac{i\pi}{2\ell^2} \frac{1}{\kappa B^2} \left[\dot{\Phi}_1(t) \sin \frac{i\pi}{2\ell}(x_1+\ell) + \dot{\Phi}_2(t) \sin \frac{i\pi}{2\ell}(\ell-x_1)\right]\right)$$

with

$$B = k^2 \alpha_n^2 + (i\pi/2\ell)^2 \tag{3}$$

and α_n are solutions of the transcendental equation

$$\alpha_n h \tan \alpha_n h = Hh \tag{4}$$

Relation (2) exhibits two terms. The first one is proportional to the applied temperatures $\Phi_1(t)$ and $\Phi_2(t)$. The second one is linearly related to the time rate $\dot{\Phi}_1(t)$ and $\dot{\Phi}_2(t)$ of the temperature perturbation.

Expression (2) has been calculated for quartz plates 2 mm thick and 2 cm long, a linear transfer such that $Hh = 50$ with equal applied temperatures ($\Phi_1(t) = \Phi_2(t) = \Phi(t)$).

Figure 3 shows the actual change of the part proportional to $\Phi(t)$ for fixed values of x_2 = 0. and 0.9 mm as a function of x_1.

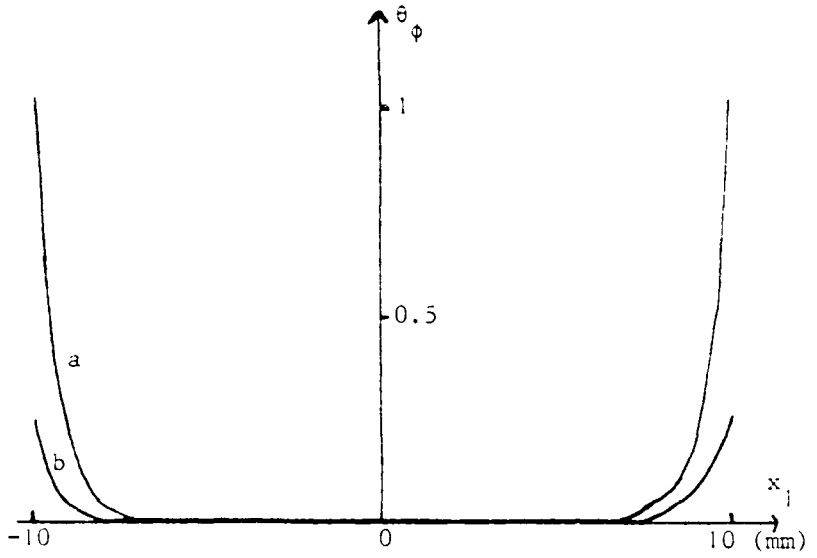

Fig. 3
a) x_2 = 0 mm
b) x_2 = 0.9 mm
Hh = 50
Y-cut

Fig. 3

Note that the temperature decreases very rapidly near to the plate ends, so that temperature variation is negligible in the interior of the plate. Furthermore, the part proportional to $\dot{\Phi}(t)$ in (2) is very small. Consequently SAW frequency changes are negligible (cf. section II).

A slight modification of this problem consists of maintaining faces at $x_2 = \pm h$ at $\Phi_1(t)$ and $\Phi_2(t)$, with thermal dissipation occuring on lateral faces. Temperature transmitted inside the plate is, to a good approximation, represented by the one dimensional model of an infinite extend plate with faces at $\Phi_1(t)$ and $\Phi_2(t)$.

Case II : Lower face heating

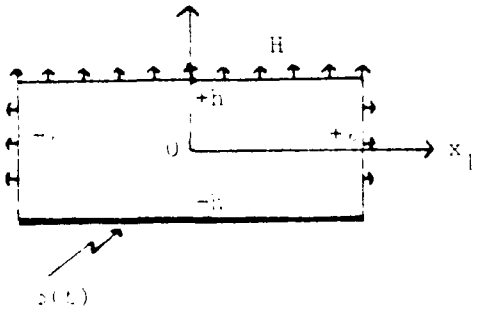

Fig. 4
Schematic diagram of the plate heating on the lower surface. Heat transfer occurs at the three other faces

It seems more interesting to study the case of prescribed temperature Φ t[illegible] on the face x_2 = -h (Fig. 4). The heat is transferred to the external medium at zero constant temperature by a linear transfer on the 3 remaining faces.

The temperature $\theta(x_1,x_2,t)$ obeys to the equations

$$\frac{\partial^2\theta}{\partial x_2^2} + \frac{\partial^2\theta}{k^2\partial x_1^2} - \frac{1}{\kappa}\frac{\partial\theta}{\partial t} = 0 \qquad -h < x_2 < h \qquad -\ell < x_1 < \ell \tag{5a}$$

$$\pm \lambda_1 \frac{\partial\theta}{\partial x_1} + H\theta = 0 \qquad x_1 = \pm \ell \qquad -h < x_2 < h \tag{5b}$$

$$\lambda_2 \frac{\partial\theta}{\partial x_2} + H\theta = 0 \qquad x_2 = +h \qquad -\ell < x_1 < \ell \tag{5c}$$

$$\theta = \Phi(t) \qquad x_2 = -h \qquad -\ell < x_1 < \ell \tag{5d}$$

Solving the equations (5) leads to the temperature distribution

$$\theta(x_1,x_2,t) = \sum_n \sum_1 2H\ell \frac{\cos k\,\alpha_n x_1}{\cos k\,\alpha_n \ell} \frac{1}{(\alpha_n^2+H^2)\ell^2 + H\ell}\frac{u_1}{2h^2} \cdot \sin\frac{u_1}{2h}(x_2+h) \,/\, (1 - \sin 2u_1/2u_1) \cdot \left(\frac{\Phi(t)}{\beta^2} - \frac{\dot{\Phi}(t)}{\kappa\beta^4}\right) \tag{6}$$

for $\quad -\ell \leq x_1 \leq +\ell$

$\quad -h < x_2 \leq +h$

with

$$\beta^2 = k^2\,\alpha_n^2 + (u_1/2h)^2 \tag{7}$$

α_n and u_1 are solutions of the transcendental equations

$$\alpha_n \ell \tan \alpha_n \ell = H\ell \tag{8}$$

$$-u_1 \operatorname{cotan} u_1 + 2hH = 0 \tag{9}$$

From relation (6), temperature $\theta(x_1,x_2,t)$ can be written as the sum of two terms, proportional respectively to $\Phi(t)$ and $\dot{\Phi}(t)$ and such that

$$\theta(x_1,x_2,t) = \theta_{\Phi}\,\Phi(t) + \theta_{\dot{\Phi}}\,\dot{\Phi}(t)$$

Charts have been prepared giving numerical values of the temperature θ. Figures 5a and 5b show θ_Φ and $\theta_{\dot{\Phi}}$ as a function of x_1 for some x_2 values. The linear transfer coefficient H has the same value as in the previous case.

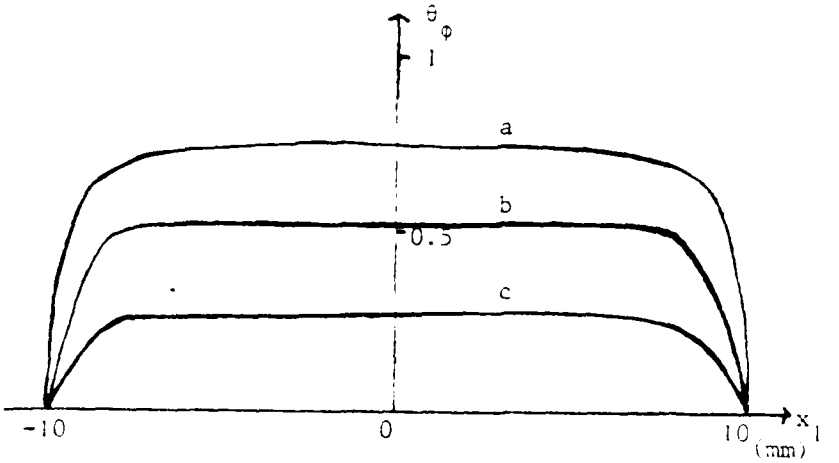

Fig. 5a

ℓ = 1 cm

h = 1 mm

a) x_2 = - 0.5 mm

b) x_2 = 0. mm

c) x_2 = + 0.5 mm

Hℓ = 500

Y cut

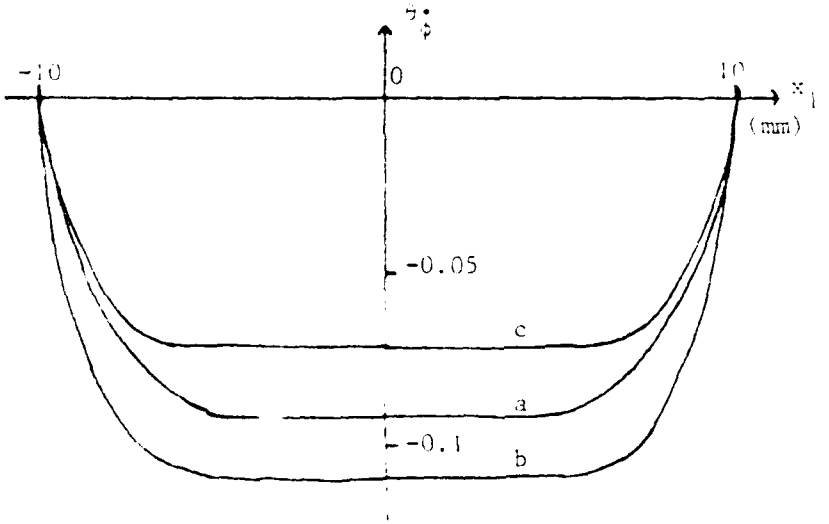

Fig. 5b

θ_Φ and θ_Φ^* as a function of x_2 are shown in Figures 6. Quantities θ_Φ and θ_Φ^* are practically constant in the main range $-x_f < x_1 < x_f$, x_f being approximately 8 mm in the case of a plate 2 cm long.

Moreover, θ_Φ is linear along the plate thickness and θ_Φ^* can be advantageously represented by a polynomial of the variable x_2 with degree 3.

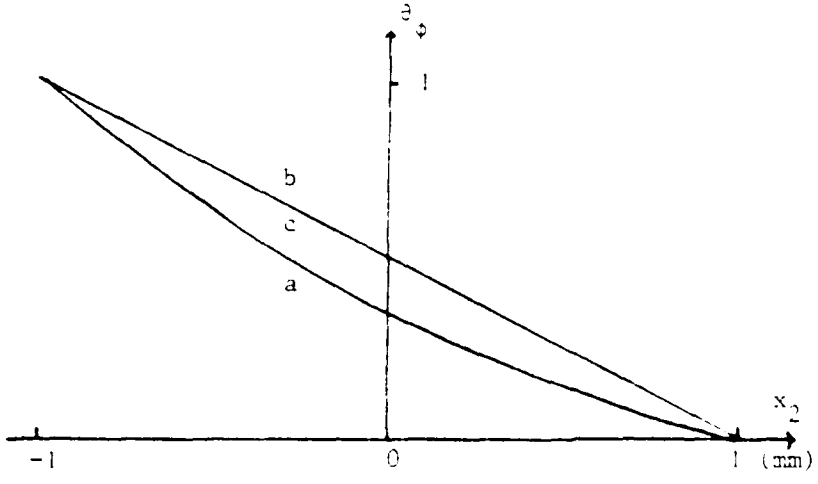

Fig. 6a

ℓ = 1 cm

h = 1 mm

a) x_1 = 9 mm

b) x_1 = 8 mm

b) x_1 = 7 mm

Hℓ = 500

Y cut

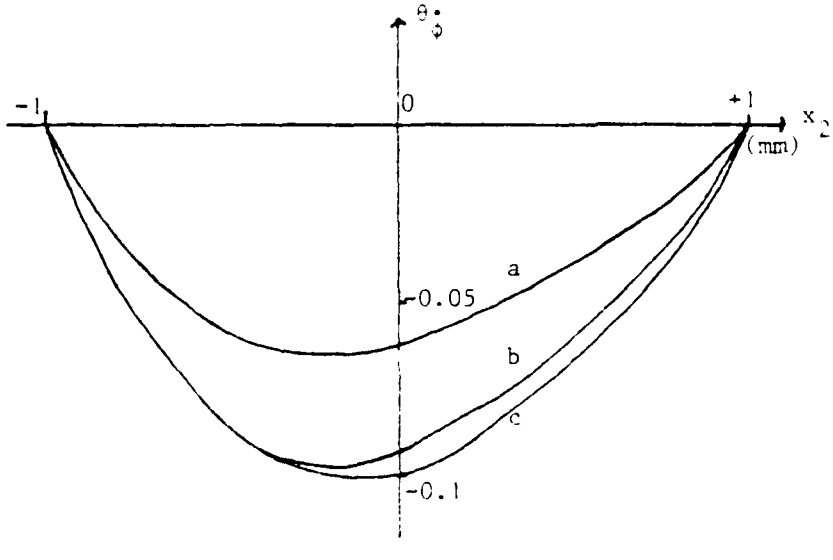

Fig. 6b

2) Two-dimensional thermal stresses in plates

Thermal stresses arise in a heated body because of the non-uniform temperature distribution and the crystalline anisotropy (at least for free plates). A two-dimensional thermoelastic problem is considered for temperature distributions of the form $\theta(x_1,x_2,t)$. For long plates, the resulting problem is plane-strain [2]

$$u_1 = u_1(x_1,x_2) \qquad u_2 = u_2(x_1,x_2) \qquad u_3 = 0 \tag{10}$$

Two-dimensional formulations

A system of approximate plate equations for the determination of thermal stresses in thin piezoelectric plates is performed by the thin plate approximation due to Mindlin [3]. Referred to the $Ox_1x_2x_3$ coordinate system, displacements u_1 are developed with respect to x_2 powers

$$\begin{aligned} u_1 &= \sum_{n=0}^{3} x_2^n \, u_1^{(n)} \\ u_2 &= \sum_{n=0}^{3} x_2^n \, u_2^{(n)} \\ u_3 &= 0 \end{aligned} \tag{11}$$

The n-th order plate strains take the following form

$$S_{ij}^{(n)} = \frac{1}{2}\left(u_{i,j}^{(n)} + u_{j,i}^{(n)} + (n+1)\left(\delta_{2\ell}\, u_k^{(n+1)} + \delta_{2k}\, u_\ell^{(n+1)}\right)\right) \tag{12}$$

and the linear thermoelastic constitutive equations are written

$$T_{ij} = C_{ijk\ell}\, S_{k\ell} - \nu_{ij}\, \theta(x_1,x_2,t) \tag{13}$$

The thermoelastic constants ν_{ij} are related to the coefficients of linear expansion $\alpha_{k\ell}$ and the elastic constants $C_{ijk\ell}$ by the usual relation

$$\nu_{ij} = C_{ijk\ell}\, \alpha_{k\ell} \tag{14}$$

The static form of Mindlin's equations may be written

$$T^{(n)}_{ij,i} - n\, T^{(n-1)}_{2j} + F^{(n)}_{j} = 0 \qquad n = 0,\ 1,\ 2 \tag{15}$$

where i takes the value 1 and skips 2 and

$$T^{(n)}_{ij} = \int_{-h}^{+h} x_2^n\, T_{ij}\, dx_2 \tag{16}$$

$$F^{(n)}_{j} = x_2^n\, T_{2j} \Big|_{-h}^{+h} \tag{17}$$

The dependence along x_3 has been disregarded.

With (12) and (13) the m-th order stress resultants take the form

$$T^{(m)}_{ij} = C_{ijk\ell} \sum_{n=0}^{2} H_{mn}\, S^{(n)}_{k\ell} - \nu_{ij}\, \theta^{(m)} \tag{18}$$

$$H_{mn} = 2h^{m+n+1} / (m+n+1) \qquad m+n \text{ even} \tag{19}$$

$$= 0 \qquad m+n \text{ odd}$$

$\theta^{(m)}$ denotes the quantities

$$\theta^{(m)} = \int_{-h}^{+h} x_2^m\, \theta(x_1, x_2, t)\, dx_2 \tag{20}$$

The boundary conditions on the main surfaces

$$T_{22}(\pm h) = 0 \qquad T_{12}(\pm h) = 0 \tag{21}$$

and on the end faces

$$T^{(n)}_{ij}(\pm \ell) = 0 \tag{22}$$

are that of a free stress plate.

Calculation of the displacements

a) Basic equations

The equilibrium equations (15) may be expressed in terms of strains by means of the strain-stress relation (18). The strains in turn can be written in terms of displacements $u_1^{(n)}$ (12).

Doubly-rotated cuts have elastic constants which introduce coupling between extension and flexure. Then, first calculations are made in the case of singly-rotated cuts, and elastic constants which couple extension and flexure are taken to vanish in the constitutive equations. So, from (15) we may write the extensional plate equations in the form

$$T_{11,1}^{(o)} = 0 \tag{23}$$

$$T_{12,1}^{(1)} - T_{22}^{(o)} = 0 \tag{24}$$

$$T_{11,1}^{(2)} - 2T_{12}^{(1)} = 0 \tag{25}$$

In these equations, the boundary conditions (21) have been taken into account so that with (17)

$$F_j^{(n)} = 0 \tag{26}$$

In the same manner, the flexural plate equations are

$$T_{12,1}^{(o)} = 0 \tag{27}$$

$$T_{11,1}^{(1)} - T_{12}^{(o)} = 0 \tag{28}$$

$$T_{12,1}^{(2)} - 2T_{22}^{(1)} = 0 \tag{29}$$

The following notation

$$u_{i,j} = \partial u_i / \partial u_j \tag{30}$$

has been used.

If relation (18) and the constitutive equations (12) are introduced in (23-25) and (27-29), displacements $u_1^{(o)}$, $u_1^{(2)}$, $u_2^{(1)}$ and $u_2^{(3)}$ on one hand are governed by the following group of equations

$$C_{11}\left(u_{1,1}^{(o)} + \frac{h^2}{3} u_{1,1}^{(2)}\right)_{,1} + C_{12}\left(u_2^{(1)} + h^2 u_2^{(3)}\right)_{,1} = \frac{\theta_{,1}^{(o)}}{2h} v_1 \tag{31}$$

$$\frac{C_{66}}{2}\left(\frac{2h^2}{3} u_1^{(3)} + \frac{h^2}{3} u_{2,1}^{(1)} + \frac{h^4}{5} u_{2,1}^{(3)}\right)_{,1} = C_{12}\left(u_{1,1}^{(o)} + \frac{h^2}{3} u_{1,1}^{(2)}\right) + C_{22}\left(u_2^{(o)} + h^2 u_2^{(2)}\right) - \frac{\theta^{(o)}}{2h} v_2 \tag{32}$$

$$C_{11}\left(\frac{h^2}{3} u_{1,1}^{(o)} + \frac{h^4}{5} u_{1,1}^{(2)}\right)_{,1} + C_{12}\left(\frac{h^2}{3} u_{2,1}^{(1)} + \frac{3h^4}{5} u_2^{(3)}\right)_{,1} - \frac{\theta_{,1}^{(2)}}{2h} v_1 = C_{66}\left(2\frac{h^2}{3} u_1^{(2)} + \frac{h^2}{3} u_{2,1}^{(1)} + \frac{h^4}{5} u_{2,1}^{(3)}\right) \tag{33}$$

and on the other hand, the flexural displacements by

$$C_{11}\left(u_{1,1}^{(1)} \frac{h^2}{3} + \frac{h^4}{5} u_{1,1}^{(3)}\right)_{,1} + C_{12} \frac{2h^2}{3} u_{2,1}^{(2)} + \frac{\theta_{,1}^{(1)}}{2h} v_1 = 0 \tag{34}$$

$$C_{66}\left(u_1^{(1)} + h^2 u_1^{(3)} + u_{2,1}^{(o)} + \frac{h^2}{3} u_{2,1}^{(2)}\right) = 0 \tag{35}$$

$$\frac{C_{66}}{2}\left(\frac{h^2}{3} u_{2,1}^{(o)} + \frac{h^4}{5} u_{2,1}^{(2)} + \frac{h^2}{3} u_1^{(1)} + \frac{h^4}{5} 3u_1^{(3)}\right)_{,1} = 2\left[C_{12}\left(\frac{h^2}{3} u_{1,1}^{(1)} + \frac{h^4}{5} u_{1,1}^{(3)}\right) + C_{22} \frac{2h^2}{3} u_2^{(2)} - \frac{\theta^{(1)}}{2h} v_2\right] \tag{36}$$

The matrix notation for C_{ijkl} has been used.

b) Free stress plate

The second order differential equations yield terms $\vartheta^{(m)}$ as known expressions in x_1. Due to the representation of the temperature as a sum of trigonometric functions (6), the solution of Eqs. (31)-(36) under conditions (22) for traction free boundaries is rather complicated.

Some simplifications can be carried out by using free stress conditions.

In order to allow for free strain $S_{22}^{(o)}$ and $S_{22}^{(2)}$ we take [3][4]

$$T_{22}^{(o)} = 0 \quad \text{and} \quad T_{22}^{(2)} = 0 \tag{37}$$

Reported in (24) this condition leads to

$$T_{12}^{(1)} = M \tag{38}$$

M is a constant which vanishes if the condition (22), $T_{12}^{(1)}(\pm\ell) = 0$, is taken into account.

From (37) and (23), (25) we obtain

$$u_{1,1}^{(o)} = \nu_1^*/C_{11}^* \frac{\theta^{(o)} h^2/5 - \theta^{(2)}/3}{8/45\ h^3} \tag{39}$$

$$u_{1,1}^{(2)} = \nu_1^*/C_{11}^* \frac{\theta^{(2)} - \theta^{(o)} h^2/3}{8/45\ h^5} \tag{40}$$

$$u_2^{(1)} = \nu_2^*/C_{22}^* \frac{\theta^{(o)} 3h^2/5 - \theta^{(2)}}{8/15\ h^3} \tag{41}$$

$$u_2^{(3)} = \nu_2^*/C_{22}^* \frac{\theta^{(2)} - \theta^{(o)} h^2/3}{8/15\ h^5} \tag{42}$$

where

$$C_{11}^* = C_{11} - C_{12}^2/C_{22} \quad ; \quad C_{22}^* = C_{22} - C_{12}^2/C_{11} \tag{43}$$

$$\nu_1^* = \nu_1 - \nu_2 \, C_{12}/C_{22} \quad ; \quad \nu_2^* = \nu_2 - \nu_1 \, C_{12}/C_{11} \tag{44}$$

Flexural equations are treated in a similar manner. Then, in order to allow for free thickness strains $S_{22}^{(1)}$, we assume

$$T_{22}^{(1)} = 0 \tag{45}$$

This leads to the flexural plate equations

$$T_{11}^{(1)} = 0 \tag{46}$$

$$T_{22}^{(1)} = 0 \tag{47}$$

$$T_{12}^{(o)} = 0 \tag{48}$$

$$T_{12}^{(2)} = 0 \tag{49}$$

and then

$$u_2^{(2)} = \frac{\theta^{(1)}}{4/3 \, h^3} \frac{\nu_2^*}{C_{22}^*} \tag{50}$$

$$u_1^{(3)} = - u_{2,1}^{(2)} / 3 \tag{51}$$

$$u_{1,1}^{(1)} = \frac{-3}{5} h^2 \, u_{1,1}^{(3)} + \frac{3}{2} \frac{\theta^{(1)}}{h^3} \frac{\nu_1^*}{C_{11}^*} \tag{52}$$

$$u_{2,1}^{(o)} = - u_1^{(1)} \tag{53}$$

When integration with respect to x_1 is performed in the above expressions, integration constants are introduced in $u_1^{(o)}$ and $u_2^{(o)}$ representing uniform translation of the plate along the x_1 axis. We can set this to zero without loss of generality. Moreover, integration constants appearing in $u_1^{(1)}$ and $u_1^{(2)}$ vanish as a consequence of conditions (21) $T_{12}^{(o)}(\pm \ell) = 0$ and $T_{12}^{(1)}(\pm \ell) = 0$.

As previously mentioned, displacements, strains and displacement gradients are obtained in a sum of trigonometric functions which is not suitable for numerical calculations.

An attempt to simplify the above expressions consists of writing the temperature distribution in a more convenient form for purposes of sensitivity calculations. This form is a polynomial obtained by polynomial regression in two dimensions (x_1 and x_2).

Polynomial representation of temperature distribution

Charts for temperature indicate that the temperature in the main part of the plate is almost constant along the x_1 direction ; the region near the end faces can be replaced by a polynomial in x_1. Consequently, without any loss of generality we may introduce the somewhat simplified temperature representation given by a polynomial, the coefficients of which are given by a polynomial regression. For the particular case of interest of figures (5) (6), θ_Φ and θ_{Φ^*} are written in the respective forms

$-0.008 \leq x_1 \leq 0$

$$\theta_\Phi = -500\,(x_2 - h) \tag{54}$$

$-0.01 \leq x_1 \leq -0.008$

$$\theta_\Phi = -(x_2 - h)(-0.0071 - 1.91x_1 - 120x_1^2)\,10^6 \tag{55}$$

$-0.006 \leq x_1 \leq 0$

$$\theta_{\Phi^*} = -0.103 + 30.5x_2 + 1.023\,10^5 x_2^2 - 31.5\,10^6 x_2^3 = F(x_2) \tag{56}$$

$-0.01 \leq x_1 \leq -0.006$

$$\theta_\Phi = F(x_2)\,[5.83 + 2330\,x_1 + 373.3\,10^3 x_1^2 + 19.85\,10^6 x_1^3] \tag{57}$$

The whole range of x_1 values is rapidly obtained. M-th order moments of θ are readily performed. Accordingly, we substitute from relations (54 - 57) into Eqs (39 - 42) and (50 - 53). Specific calculations have been made for quartz plates 2. mm thick and 2. cm long and compared to the general calculations performed without approximations.

SENSITIVITY OF SAW TO TEMPERATURE GRADIENTS

1) Calculations of sensitivities

When a quartz resonator undergoes heating, two kinds of effects affect the natural frequency : a direct thermal effect by means of dilatation and material temperature coefficients like αC_{ijkl}, and an indirect thermoelastic effect induced by nonlinearities of the quartz crystal.

Both effects can be considered as a bias applied on the crystal substrate which modifies the second order elastic constants (C_{ijkm} become $\overline{A_{ijkm}}$). In natural state coordinate system [6] the nonlinear propagation equation is written

$$\rho_o u_{i,tt} = (\overline{A_{ikjm}} u_{j,m})_{,k} \qquad (58)$$

where ρ_o is the specific mass and u_j the displacement due to the high frequency vibrations.

The boundary conditions corresponding to a stress free surface are

$$\overline{A_{ikjm}} u_{j,m} = 0 \quad \text{for} \quad x_2 = 0 \qquad (59)$$

$\overline{A_{ikjm}}$ are the modified elastic constants, which can be written in the form

$$\overline{A_{ikjm}} = C_{ikjm} + \overline{H_{ikjm}} \qquad (60)$$

where the $\overline{H_{ikjm}}$ tensor is considered as a small term with respect to the second order elastic constant C_{ikjm}. It can be related to the temperature and the thermal stresses and strains in the following way

$$\overline{H_{ikjm}} = \delta_{ij}\overline{t_{km}} + \overline{U_{i,p}}C_{kpmj} + \overline{U_{j,q}}C_{kimq} + \overline{S_{uv}}C_{kmquv} + \alpha C_{ikjm} C_{ikjm}\,\theta(x_2,t) \qquad (61)$$

where $\overline{t_{km}}$, $\overline{S_{uv}}$ and $\overline{U_{i,p}}$ are respectively the thermodynamic tensions, the deformations and the displacement gradients induced by temperature.

In the case of SAW oscillators, the nonlinear coupling of the crystal with the high frequency wave depends on its depth penetration. Then perturbation terms $\overline{H_{ikjm}}$ are a function of the step variable x_2 and can be written following the relation

$$\overline{H_{ikjm}} = \sum_n \overline{\alpha_{ikjm}^{(n)}}\, x_2^n \qquad (62)$$

By using a perturbation method [5][6], relative frequency shifts are calculated

$$\frac{\Delta\omega}{\omega_o} = \frac{\sum_n \sum_{p,q} \frac{A_p\, {}^{o}u_j^{o}(p)\; A_q^{*}\, {}^{o}u_i^{o}(q)^{*}\; n_m^{(p)}\; n_k^{(q)*}}{q_p - q_q^{*}} \cdot \frac{n!\;\overline{\alpha_{ikjm}}^{(n)}}{\left(\frac{\omega_o}{V_o}\right)^{n} (q_p - q_q^{*})^{n}}}{2\, \rho_o\, V_o^2 \sum_{p,q} \frac{A_p\, {}^{o}u_\ell^{o}(p)\; A_q^{*}\, {}^{o}u_\ell^{o}(q)^{*}}{q_p - q_q^{*}}} \qquad (63)$$

A_s, ${}^{o}u_k^{o}(s)$, $n_r^{(s)}$ and q_s are characteristic quantities of surface acoustic waves propagating in a nonperturbed medium

$${}^{o}u_k = \sum_s A_s\, {}^{o}u_k^{o}(s)\; e^{j\omega_o\left(t - \frac{n_r^{(s)}\, x_r}{V_o}\right)} \qquad (64)$$

Since the temperature distribution is proportional partly to $\Phi(t)$ and partly to the time derivative $\dot{\Phi}(t)$ (see Eq. 6 of previous section for example) the perturbation terms $\overline{H_{ikjm}}$ have two parts

$$\overline{H_{ikjm}} = \overline{a_{ikjm}}\,\Phi(t) + \overline{b_{ikjm}}\,\dot{\Phi}(t) \qquad (65)$$

Relative frequency shifts $\Delta\omega/\omega_o$ are calculated for $\Phi(t)$ and $\dot{\Phi}(t)$ contributions

$$\frac{1}{\Phi(t)}\frac{\Delta\omega}{\omega_o} = \bar{a} \quad \text{and} \quad \frac{1}{\dot{\Phi}(t)}\frac{\Delta\omega}{\omega_o} = \tilde{a} \qquad (66)$$

Then, when a SAW oscillator is submitted to temperature variations, such as fast fluctuations of temperature superimposed on slow temperature changes, relative frequency shifts are written

$$\boxed{\frac{\Delta\omega}{\omega_o} = a_o\,[T - T_o] + a_o\,[T - T_o]^2 + a_o\,[T - T_o]^3 + \bar{a}\,\dot{T}(t) + \tilde{a}\,\ddot{T}(t)} \qquad (67)$$

where a_1, a_2 and a_3 are respectively the first, second and third order temperature coefficients of the frequency calculated or measured in the case of static thermal behavior and T_o is the reference temperature.

Some comments about coefficients appearing in Eq. 67 may be given

- coefficients a_o, b_o, c_o describe the thermal behavior of the quartz when it experiences a homogeneous temperature variation given by T.

- $\bar{a}$-coefficient determines the frequency change resulting from a local temperature perturbation Φ which could be time-dependent or time-independent. This local temperature perturbation induces in the plate an inhomogeneous temperature repartition followed by stresses and strains. This leads to new properties of the deformed crystal reflected by $\overline{H_{ikjm}}$ terms (in the place of C_{ikjm}).

- $\tilde{a}$-coefficient is related to the time rate of change of the perturbation and its effect vanishes when aforementioned rates become negligible.

Frequency shifts for singly rotated cuts

Coefficients $\bar{a}$ and $\tilde{a}$ defined in relation (66) have been evaluated in the following cases (see Fig. 4)

- Time varying temperature $\Phi(t)$ is applied on the lower surface of the plate
- Some linear heat transfer H occurs on the other sides of the plate.

Results obtained by the two dimensional model are shown in Table 1. The normalized transfer coefficient χH is equal to 500.

cut	Y, X	AT, X	ST, X
$\bar{a}_D$ (ppm/K)	0.09	0.06	0.067
$\tilde{a}_D$ (μs/K)	-0.11	-0.10	-0.09
$\bar{a}_p$ (ppm/K)	0.096	0.065	0.07
$\tilde{a}_p$ (μs/K)	-0.13	-0.13	-0.11

Table 1

Theoretical values of $\bar{a}$ and $\tilde{a}$ for singly rotated cuts

Coefficients $\bar{a}_D$ and $\tilde{a}_D$ result from numerical calculation of dynamic thermal sensitivity in which temperature distribution is given as the general solution of the thermal diffusion equation (see Eq. 6).

Coefficients $\bar{a}_p$ and $\tilde{a}_p$ are calculated in the same way but the temperature distribution is replaced by the polynomial expansion obtained by polynomial regression in two dimensions as indicated in the former section (see Eqs. 54-57).

Comparison between $\bar{a}_D$ and $\bar{a}_p$ coefficients on one hand and $\tilde{a}_D$ and $\tilde{a}_p$ coefficients on the other hand shows that for each cut obtained values are in good agreement and it seems reasonable to use a simplified représentation for the 2-dimensional temperature.

It appears that $\bar{a}$-coefficients are weak and their influence on the static behavior is not important.

From an experimental point of view, measured values of dynamic coefficients of SAW devices do not validate the adequacy of the two-dimensional model. Nevertheless, we present a simulation of frequency temperature curves.

2) Simulation of the dynamic thermal behavior

From Table 1, frequency-temperature characteristics were calculated for Y-cut, ST-cut, AT-cut for some time rates of change of temperature.

a) Y-cut, X propagation

$$\frac{\Delta f}{f}(T) = 24.3\ 10^{-6}(T-T_o) + 18.7\ 10^{-9}(T-T_o)^2 + 0.091\ 10^{-6}\ \Phi(t) - 0.11\ 10^{-6}\ \dot{\Phi}(t)$$

$T_o = 25\ ^\circ C$: $\Delta T = .1\ ^\circ C$ and $\Phi(t) = \Delta T \sin \Omega t$

$$\dot{\Phi}(t) = \Delta T.\Omega \cos \Omega t$$

where Ω is related to the time varying rate v of the temperature by

$$v = \frac{dT}{dt} = \Omega \ .\ \Delta T$$

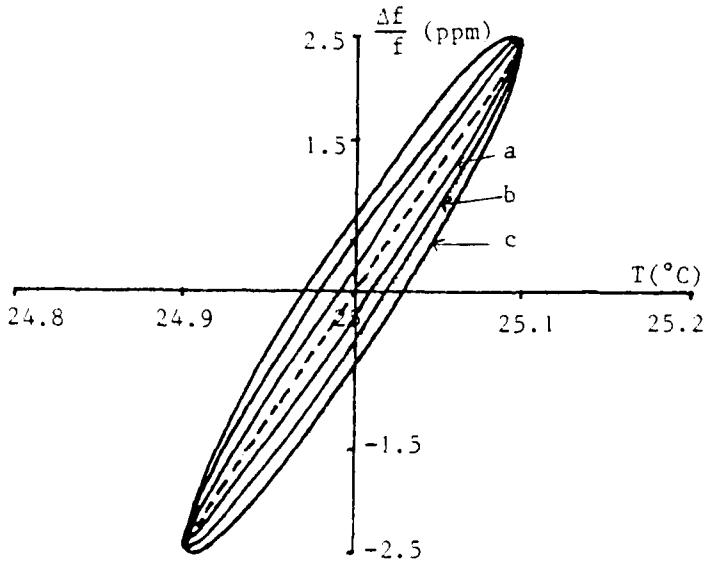

ΔT = .1 °C

a) v = 130 K/mn

b) v = 260 K/mn

c) v = 390 K/mn

Velocity values are large and experimentally not realistic. That means that the Y-cut is very insensitive to temperature gradients compared to its static thermal behavior.

Fig. 7 : Theoretical dynamic thermal behavior of Y-cut. Dashed line is the static frequency temperature characteristic.

b) AT-cut, X-propagation

Static frequency-temperature characteristic of the AT,X-cut presents a turnover point at 65.2 °C. Temperature gradients introduce a drift of the turnover point due to the $\bar{a}$-coefficient. For the AT-cut, $\bar{a}$-coefficient is equal to 0.06 $10^{-6}/°K$ which would correspond to a new turnover point at 65.9 °C.

Dynamical thermal behavior of the AT-cut is computer-simulated around this new turnover point for several temperature variation velocities

$$\frac{\Delta f}{f} = 3.3\ 10^{-6}(T-T_o) - 41\ 10^{-9}(T-T_o)^2 + 0.06\ 10^{-6}\ \Phi(t) - 0.10\ 10^{-6}\ \dot{\Phi}(t)$$

with : $\Phi(t) = \Delta T \sin \Omega t$

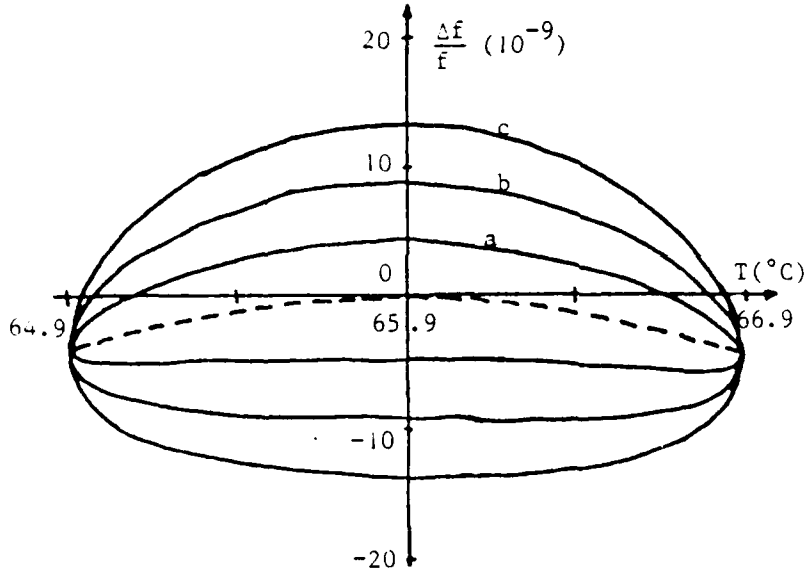

T_o = 25 °C
ΔT = 1 °C

a) v = 13 K/mn
b) v = 26 K/mn
c) v = 39 K/mn

Fig. 8 : Theoretical dynamic thermal behavior of AT,X cut
Dotted line is the static frequency temperature characteristic around the new turnover point (65.9 °C)

c) ST-cut, X-propagation

The turnover point of the static frequency temperature characteristic of the ST-cut is at 25 °C. As for the AT-cut, the $\Phi(t)$ term leads to a new turnover point at a temperature of 25.8 °C.

Computer simulation is made around this peculiar temperature value for several temperature variation velocities and curves are plotted in Fig. 9.

Thermal behavior of the ST-cut, X propagation is described by the following relation taking into account both static and dynamic effects

$$\frac{\Delta f}{f} = -39.6\ 10^{-9}(T-T_o)^2 + 58.3\ 10^{-12}(T-T_o)^3 + 0.067\ 10^{-6}\ \Phi(t) - 0.09\ 10^{-6}\ \dot{\Phi}(t)$$

with : $\Phi(t) = \Delta T \sin \Omega t$

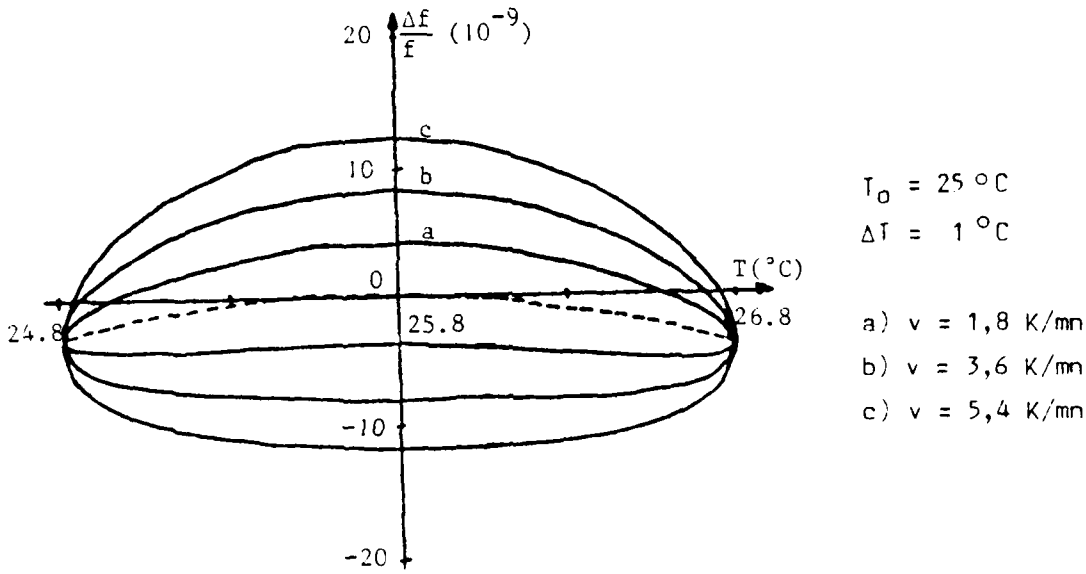

Fig. 9 : Theoretical dynamic thermal behavior of ST,X cut around the new turnover point (25.8 °C)

Frequency shifts for a doubly rotated cut - FST-cut

In the case of singly-rotated cuts, terms in constitutive equations which couple extension and flexure are vanishing. In doubly-rotated cut calculations, these terms are to be included in equations. Although the previous two-dimensional stress calculations are not adequate for doubly-rotated cuts, we still assume that the assumptions used in our calculations hold for the FST-cut ($\Phi = 6^\circ 20'$, $\Theta = -41^\circ 30'$ and $\Psi = 26^\circ$) and corresponding results of sensitivities are presented in Table 2.

FST-cut	Calculations by analytical expressions (D)	Calculations by polynomial representation (p)
$\bar{a}$ (ppm/K)	0.17	0.15
$\tilde{a}$ (μs/K)	0.06	0.09

Table 2

Theoretical values of $\bar{a}$ and $\tilde{a}$ for FST-cut

To illustrate dynamic thermal behavior of the FST-cut, computer simulation was performed around the new turnover point σ_o = 29.2 °C. Results are shown in Fig. 10.

$$\frac{\Delta f}{f} = -\ 20\ 10^{-9}(T-T_o)^2 + 10\ 10^{-12}(T-T_o)^3 + 0.17\ 10^{-6}\ \Phi(t) + 0.06\ 10^{-6}\ \Phi(t)$$

with : $\Phi(t) = \Delta T \sin \Omega t$

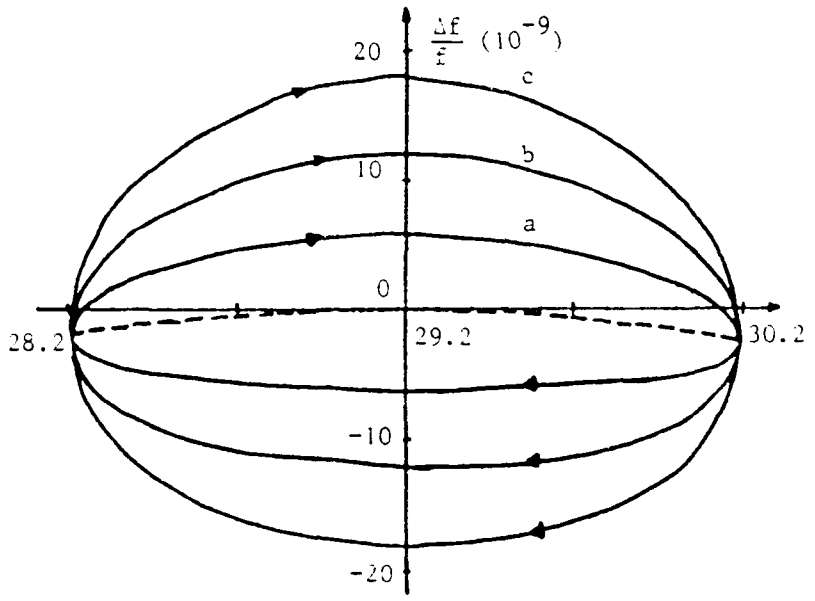

T_o = 25 °C
ΔT = 1 °C

a) v = 5 K/mn
b) v = 10 K/mn
c) v = 15 K/mn

Fig.10 : Theoretical simulation of dynamic thermal behavior of the FST-cut. Dotted line is the static frequency-temperature characteristic around the new turnover point (29.2 °C)

In conclusion, the FST-cut exhibits sensitivity to time-varying temperatures of the same order of magnitude as for singly rotated cuts, despite the fact that the model neglects terms coupling extension and flexure.

GENERAL CONCLUSION

The stress state caused in quartz crystal by thermal perturbation has been analyzed for its effects on the temperature stability of SAW devices. A two-dimensionnal model was developed in order to obtain first ; temperature distributions which are presented as temperature charts, and second ; stresses induced by thermal effects.

Corresponding dynamic sensitivity was obtained by a perturbation method and characterized by two coefficients, the first one $\bar{a}$, directly related to thermal strain state, the second one $\tilde{a}$ reflecting the response to time rate changes of the temperature.

Computer simulations of dynamic thermal behavior are made for singly rotated cuts (Y, AT, ST-cuts, X propagation) and the FST-cut and for several values of temperature time rates. We note the small dynamic thermal sensitivity of these cuts where $\tilde{a}$ is smaller than $\tilde{a}$ measured for SC-cut bulk wave resonators. We also have discussed the expected impact of dynamic coefficients on the frequency-temperature characteristics.

It should be noted that theoretical $\bar{a}$ and $\tilde{a}$ coefficients are derived in the restrictive case of a free plate. Accordingly, mechanical stresses induced by the external mounting have been ignored in this treatment. The description must be extended to incorporate effects such as forces due to the differential expansion between mounting and plate. The specification of prescribed boundary conditions in any experimental situation is a peculiar problem and, in many cases, its solution may require a three dimensional model.

At this point, only few experimental results on dynamical temperature effect in SAW devices are reported in the literature. To confirm the validity of the theoretical model, experimental values for several cuts must be obtained. Consequently, it is necessary to consider dynamic thermal experimental implications for SAW oscillators built in the same technology.

Systematic experiments must be performed to move forward on this problem.

As a brief summary, the following points form the main results of this program :

- dynamic thermal behavior of SAW devices is due to direct influence of temperature gradients and to stresses induced by thermoelastic properties inside the free plate.
- theoretical dynamic temperature coefficients of SAW devices are smaller than those measured in SC-cut bulk wave resonators (1 to 5 10^{-7} s/K).
- mechanical stresses due to the mounting have to be included to model completely the thermal behavior of SAW oscillators.
- systematic measurements are necessary to confirm theoretical results obtained during this program.

REFERENCES

(1) H. Carslaw and J. Jaeger, "Conduction of heat in solids", Oxford University Press, London (1959).

(2) B.A. Boley and J.H. Werner, "Theory of thermal stresses", John Wiley and Sons (1960).

(3) R.D. Mindlin, "An introduction to the mathematical theory of vibrations of elastic plates", Monograph USASCEL, Fort Monmouth, N.J. (1955).

(4) H.F. Tiersten, B.K. Sinha and T.R. Meeker, J. Appl. Phys., 52(9), p. 5614 (1981).

(5) M. Planat, D. Hauden, "Nonlinear properties of bulk and surface acoustic waves in piezoelectric crystals", Ferroelectrics, vol. 42, pp. 117-136, (1982).

(6) H.F. Tiersten, "Perturbation theory for linear electroelastic equations for small fields superposed on a bias", J. Acoust. Soc. Am., 64, p. 832, (1978).

MISSION
of
Rome Air Development Center

RADC plans and executes research, development, test and selected acquisition programs in support of Command, Control Communications and Intelligence (C^3I) activities. Technical and engineering support within areas of technical competence is provided to ESD Program Offices (POs) and other ESD elements. The principal technical mission areas are communications, electromagnetic guidance and control, surveillance of ground and aerospace objects, intelligence data collection and handling, information system technology, solid state sciences, electromagnetics and electronic reliability, maintainability and compatibility.

Printed by
United States Air Force
Hanscom AFB, Mass. 01731

END

FILMED

2-85

DTIC